Coastal Engineering 161 (2020) 103750

Contents lists available at ScienceDirect

Coastal Engineering

journal homepage: http://www.elsevier.com/locate/coastaleng

Operational monitoring and forecasting of wave run-up on seawalls

Ching-Jer Huang [a,b,*], Yu-Cheng Chang [a], Shih-Chieh Tai [a], Chun-Yuan Lin [b], Yen-Pin Lin [b], Yang-Ming Fan [b], Chi-Min Chiu [b], Li-Chung Wu [b]

[a] Department of Hydraulic and Ocean Engineering, National Cheng Kung University, Tainan, 70101, Taiwan, ROC
[b] Coastal Ocean Monitoring Center, National Cheng Kung University, Tainan, 70101, Taiwan, ROC

ARTICLE INFO

Keywords:
Operational monitoring and forecasting
Wave run-up and overtopping
Seawall
Empirical formulas
Multi-model ensemble approach

ABSTRACT

In this work, a wave run-up monitoring system and a model for forecasting the wave run-up height on a seawall were developed. Electrical conductivity sensors were installed on the seaward slopes of seawalls to measure the wave run-up heights. The general packet radio service protocol was used to transmit the measured data in real time to the desired remote location. The Princeton Ocean Model and WAVEWATCH III were used to predict the water levels and ocean waves, respectively, by using the available wind fields. The empirical formulas recommended in the Coastal Engineering Manual (2011) and EurOtop (2018) were adopted to estimate the run-up height. The wave run-up heights were forecasted 72 h in advance and were renewed at 6-h intervals as new wind fields became available. The developed monitoring system and forecasting model were combined for operational monitoring and forecasting of wave run-up on seawalls. The wave run-up monitoring system was set up at three seawalls along the southwestern coast of Taiwan from 2013 to 2016. Consistency between the forecasted and measured wave run-up heights during typhoon periods demonstrated the feasibility of using the proposed method for monitoring and forecasting wave run-up heights. Furthermore, the multi-model ensemble approach was adopted to improve the unsatisfactory run-up forecasting performance during typhoon periods, and the forecasted run-up heights were eventually presented as a band with upper and lower limits as opposed to single values. The forecast results can be used to provide advance warning of possible wave overtopping and associated coastal flooding during typhoon periods.

1. Introduction

Wave run-up and overtopping on seawalls have been investigated extensively. The wave run-up height, which is sometimes referred to as the wave run-up level, is defined as the vertical distance between the still water level and the intersection of the seawall slope and the highest water surface level. When the maximum run-up level exceeds the seawall crest level, overtopping occurs, which may cause coastal flooding. For this reason, predicting and forecasting of wave run-up height and mean overtopping discharge during typhoon or storm periods are critical because they provide early warning of possible coastal flooding, which can potentially cause structural failures and losses of property and lives. In the design of coastal structures, in addition to the mean overtopping discharge (m^3/s per m width, or often *liters*/ s per m width), the maximum overtopping volume (*liters* per m width) during a storm event should also be considered (EurOtop, 2018).

Wave run-up on a sloping beach or on a seawall has been studied widely by using analytical methods (Carrier and Greenspan, 1958; Synolakis, 1987; Pritchrad et al., 2008), numerical modeling (Kennedy et al., 2000; Hubbard and Dodd, 2002; Lynett et al., 2002; Bradford, 2011; Ruju et al., 2014; Fiedler et al., 2018, among many others), field measurements (Troch et al., 1998; Van Gent, 2001; De Rouck et al., 2007; Na et al., 2011; Yoo et al., 2013; Fiedler et al., 2015; Wenneker et al., 2016; Atkinson et al., 2017), and laboratory experiments (Hall and Watts, 1953; Saville, 1956; Raichlen and Hammack, 1974; Mase, 1989; Van der Meer and Stam, 1992; Van der Meer, 1998; Hsiao et al., 2008, among many others). In the early stages of laboratory research on this topic, Hall and Watts (1953) conducted experiments to study the run-up of solitary waves on impermeable slopes. Saville (1956) performed a series of experiments to study the run-up of regular waves on various test structures, namely vertical, curved, step-faced, and riprap-faced walls. Based on the experimental results of Saville (1956), Hunt (1959) proposed an empirical formula relating run-up height to incident wave height. Raichlen and Hammack (1974) conducted experiments to

* Corresponding author. Department of Hydraulic and Ocean Engineering, National Cheng Kung University, No. 1, University Road, Tainan, 70101, Taiwan, ROC.
E-mail address: cjhuang@mail.ncku.edu.tw (C.-J. Huang).

https://doi.org/10.1016/j.coastaleng.2020.103750
Received 12 September 2019; Received in revised form 19 May 2020; Accepted 20 June 2020
Available online 9 July 2020
0378-3839/

investigate the effect of incident wave parameters on run-up height for both smooth-faced and armor-faced structures. In their experimental results, the maximum run-up heights for both smooth and armored slopes were always greater than the run-up heights obtained for waves that break at the toe of the structure.

Ocean waves are irregular. The run-up heights obtained under regular wave conditions may not be applicable to real seawalls. For more practical applications, Mase (1989) conducted comprehensive laboratory experiments to derive a formula for predicting the run-up elevation of random waves on gentle, smooth, and impermeable slopes. Van der Meer and Stam (1992) investigated the run-up of irregular waves on rock slopes, including revetments and breakwater structures. Empirical formulas for wave run-up heights on both smooth and rock slopes were presented on the basis of large-scale laboratory tests.

Based on the results of a series of laboratory experiments, De Waal and Van der Meer (1992) proposed empirical formulas for determining wave run-up height and overtopping discharge on seawalls. Significant factors involved in the formulas included the type of seawall, roughness of the seawall, type of slope, water depth, and incident wave conditions. Van der Meer (1998) conducted large-scale laboratory tests to investigate wave run-up and overtopping on dikes. On the basis of the test results, they proposed an empirical formula for use in dike design to prevent storm surge flooding. The test results demonstrated that the roughness of the seawall slope plays an important role in preventing wave overtopping. Hughes (2004) examined available run-up data of regular, irregular, and solitary waves on smooth and impermeable slopes by using the wave momentum flux parameter to derive a new wave run-up formula. Hsiao et al. (2008) conducted laboratory experiments in a huge wave flume ($300\ m \times 5\ m \times 5.2\ m$) to investigate the evolution of breaking solitary waves on a mildly sloping beach. They proposed a formula for predicting the maximum run-up height of a breaking solitary wave on a plane beach with a wide range of beach slope.

Various empirical formulas for determining wave run-up height and overtopping discharge on seawalls are provided in the Coastal Engineering Manual (2011), European Overtopping Manual (EurOtop, 2018), and Technical Advisory Committee for Flood Defense in The Netherlands (TAW, 2002).

Field measurements of wave run-up on natural beaches and seawalls have also been conducted. Long-term field measurements (1994–2003) have been performed at the Petten site in the Netherlands (Hordijk, 2004; Wenneker et al., 2016) to obtain field data on (i) wave propagation from deep water through the surf zone to the dike, (ii) wave run-up on the Petten sea dike (a smooth impermeable dike), and (iii) wave overtopping. The wave run-up gauge consisted of two combined step gauges and was placed in the dike revetment. An empirical wave run-up formula based on gathered field run-up data was published in TAW (2002) and EurOtop (2007). The field run-up data revealed that the long-period waves cause an increase in wave run-up height with respect to situation without heavy wave breaking. Collaborations with other hydraulic laboratories revealed that for an impermeable dike, run-up data obtained from 2D and 3D small-scale model tests agree with field measurement results. Van Gent (2001) performed prototype measurements on the Petten sea dike, physical model tests, and numerical model computations to study wave run-up on dikes with shallow foreshores. Both numerical model computations and physical model tests supported the use of a special spectral wave period, referred to as $T_{m-1,0}$, at the toe of coastal structures to describe wave run-up for single- and double-peaked spectra. Furthermore, a formula was proposed for estimating wave run-up on coastal structures with shallow foreshores or with relatively deep water at the toe of coastal structures. Troch et al. (1998) reported on the prototype monitoring system at Zeebrugge harbor in Belgium that was established to acquire field data on waves interacting with a rubble mound breakwater. Both pore pressure sensors and vertically placed step gauges were installed to measure internal pore pressure in the breakwater and wave run-up and run-down, respectively. Non-dimensional wave run-up heights and wave run-down heights as a function of the Iribarren number were obtained and calibrated with the run-up formula proposed by Losada and Giménez-Curto (1982). De Rouck et al. (2007) studied wave run-up by performing both field measurements on the Zeebrugge rubble mound breakwater and small-scale model tests in various hydraulics laboratories. Wave run-up was measured using a digital run-up gauge. Their results revealed that wave run-up is underestimated in small-scale models and the porosity of the armor layer significantly influences wave run-up.

Na et al. (2011) proposed a method to forecast the wave run-up scale on coastal structures based on a multiple linear regression of the wave run-up scale and offshore wind and wave parameters. The wave run-up scale, describing primarily the relative height of run-up to the crest elevation of the breakwater, was obtained from long-term visual observations, whereas the offshore wind and wave data were obtained from models. Yoo et al. (2013) investigated wave run-up on a seaward slope in the field by using optical video imagery and compared the test data with those obtained using an empirical formula.

Atkinson et al. (2017) assessed the accuracy of 11 run-up models against field data collected under moderate wave conditions from 11 largely planar beaches along southeast Australia. Wave run-up heights were obtained by analyzing video images. The authors demonstrated that no single model provides optimal predictions for all studied beaches and the most appropriate models for predicting run-up values in the field are those developed from field data. Pillai et al. (2019) proposed a formula for wave run-up on bermed coastal structures by conducting physical model tests and collecting existing data. In physical model tests, wave run-up was obtained by analyzing images collected from digital video cameras for approximately 1000 waves for each test condition. The new formula was validated using field measurements obtained by Van Gent (2001) on the Petten sea dike.

In recent studies on wave run-up on a natural beach (Stockdon et al., 2006; Senechal et al., 2011; Ruju et al., 2014; Fiedler et al., 2015, 2018), in addition to measurement of the run-up height, the steady and time-varying components of wave run-up were revealed in detail. The steady component, referred to as wave setup, is the additional elevation of water level driven by gradients in the wave-induced mean momentum flux produced by breaking waves in shallow water (Longuet-Higgins and Stewart, 1964). The oscillating component, termed swash fluctuation, is driven by the part of wave energy that is not dissipated by breaking waves, and it has been investigated by separating it into the infragravity band (0.004–0.04 Hz) and sea-swell (0.04–0.25 Hz) (Fiedler et al., 2018). Notably, the wave setup has been included in the wave run-up measurements.

To mitigate possible coastal disasters, estimating the maximum wave run-up height and the overtopping discharge during storm conditions is critical. However, few field tests of wave run-up on a real seawall, especially under storm conditions, have been conducted, and comparisons of field test data with the data estimated using available empirical formulas are rare. Operational real-time monitoring and forecasting of wave run-up and overtopping on a real seawall are indispensable for providing advance warning of possible coastal hazards, especially on an island such as Taiwan, which is hit by three to four typhoons on average each year. For example, in 2012, during the period of typhoon Talim, the wave overtopping on the Tsen-Wen seawall in southern Taiwan scoured the vegetation-covered lee side of seawall and subsequently dislodged its soil core. This led to damage to the seaward slope caused by the wave's impact. Although a concrete seawall was rebuilt in early 2013, local residents remain concerned regarding the possibility of coastal flooding during the next typhoon.

In this study, an operational real-time monitoring and forecasting system for wave run-up on a real seawall is developed. The system can be set up on any seawall in coastal areas to provide early warning signals about possible wave overtopping, which may cause coastal flooding. The Princeton Ocean Model (POM) and WAVEWATCH III (WWIII) are used to predict the water levels and ocean waves, respectively, from

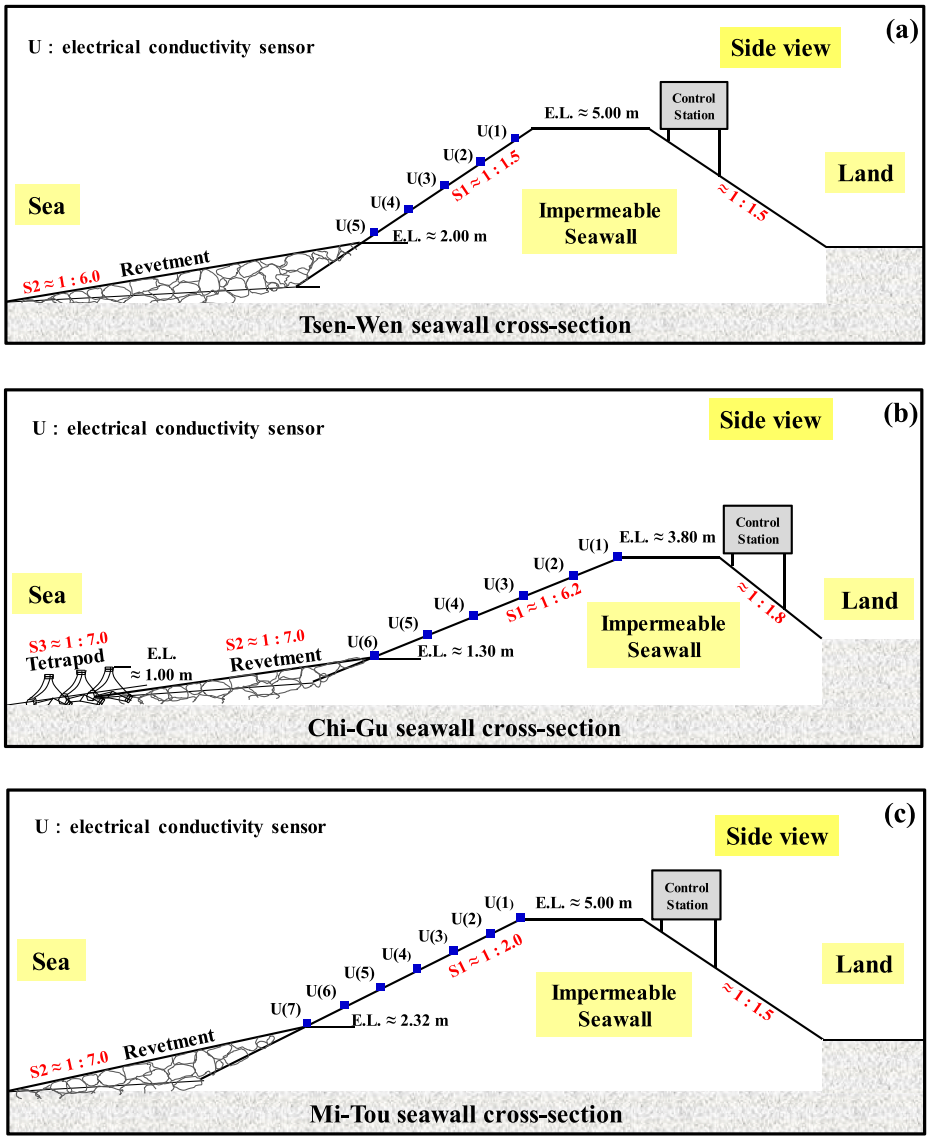

Fig. 1. Setup of the wave run-up monitoring system on the seawalls; (a) Tsen-Wen seawall, (b) Chi-Gu seawall, and (c) Mi-Tou seawall. The electrical conductivity sensors were used as run-up sensors and installed on the seaward slopes of the seawalls.

forecasted wind fields. When the water levels and offshore wave conditions are known, the empirical formulas for wave transformation and wave run-up height are used to estimate the wave height at the toe of the seawall and the wave run-up height on the seawall. The monitoring and forecasting of overtopping discharge on a real seawall are also important. However, because seawalls in Taiwan are usually built tall, the occurrence of overtopping is rare even during typhoon periods. Therefore, this study focuses only on wave run-up. Detailed studies of wave overtopping on seawalls can be found in Losada et al. (2008) and EurOtop (2018).

The remainder of this paper is organized as follows. Section 2 presents the proposed real-time wave run-up monitoring system. The model for forecasting wave run-up on a real seawall is presented in Section 3. Section 4 compares the forecasted and measured wave run-up heights obtained during various typhoons that have hit Taiwan. Finally, the conclusions of this study are given in Section 5.

2. Wave run-up monitoring system on a seawall

In this study, an operational wave run-up monitoring system that can provide real-time data about wave run-up heights on a seawall was developed. The measured wave run-up height data can be used to provide an advance warning signal of possible wave overtopping. In addition, the measured values can be used to calibrate the unknown coefficient involved in the empirical formula for determining wave run-up on a seawall, which is the roughness factor for the tetrapod section of the seawall.

Fig. 1 is a schematic of the setup of the wave run-up monitoring system on the seawalls studied in this work, namely the Tsen-Wen, Chi-Gu, and Mi-Tou seawalls. Five to seven high-precision run-up gauges were mounted on the seaward slopes of these seawalls. Electrical conductivity sensors were used as the wave run-up sensors. Each wave run-up sensor consisted of a conductivity sensor (EC-200) and a conductivity controller (EC-106); both devices were manufactured by HOTEC Instruments Co., Ltd., Taiwan. The working temperature of the conductivity sensor was $0-80\ ^{o}C$. Therefore, it could withstand the high temperatures (around $40\ ^{o}C$) during the summer in Taiwan. The measurement range of the conductivity sensor was 0–200,000 $\mu S/cm$ (micro-Siemens per centimeter, 1 $\mu S/cm = 0.64$ ppm). In general, the conductivity of freshwater is lower than 1,200 $\mu S/cm$ (rainwater at $25\ ^{o}C$, 50 $\mu S/cm$), and that of seawater is 48,000–52,000 $\mu S/cm$ (31–34 ppt). On the lee side of the seawalls, a control station was set up to house the

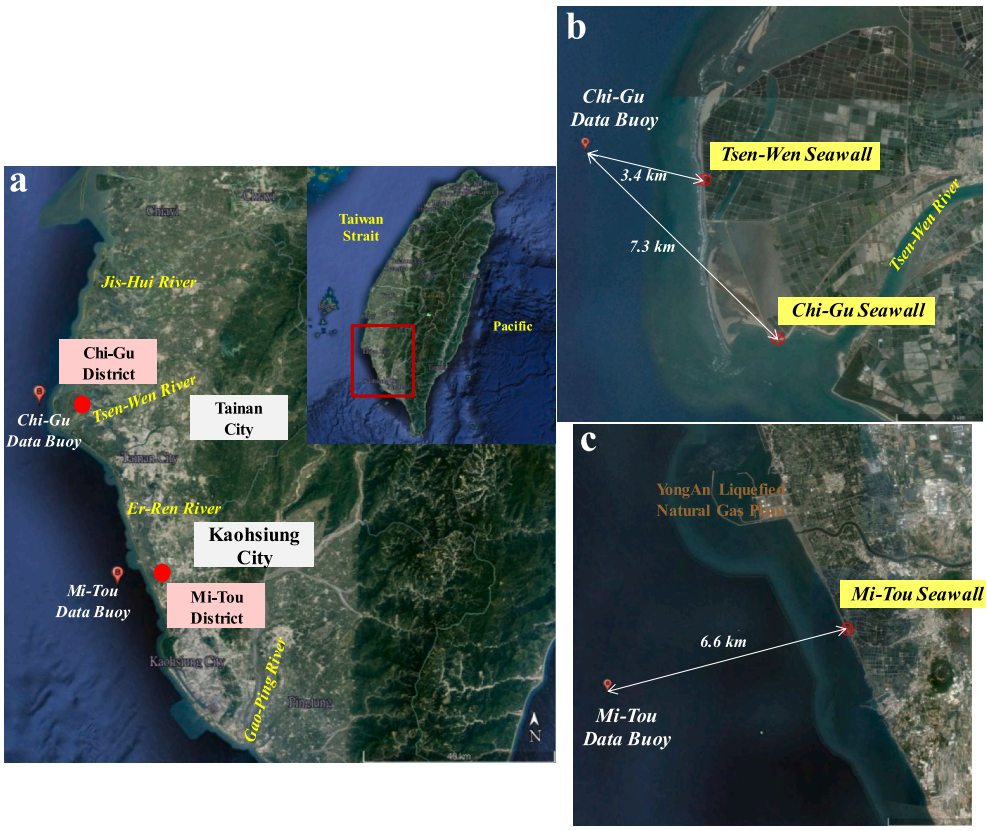

Fig. 2. (a) Map of the island of Taiwan and the locations of Chi-Gu and Mi-Tou districts and data buoys. (b) Detailed map of the Tsen-Wen and Chi-Gu seawalls located in the Chi-Gu district, Tainan City. The Chi-Gu buoy is on the northwestern side of the Tsen-Wen and Chi-Gu seawalls. (c) Detailed map of the Mi-Tou seawall in the Mi-Tou district, Kaohsiung City. The Mi-Tou buoy is on the southwestern side of the Mi-Tou seawall. Operational wave run-up monitoring systems were installed at the Tsen-Wen, Chi-Gu, and Mi-Tou seawalls.

Table 1
Parameters involved in the empirical formulas for determining the wave run-up height on the seawall.

Parameter	Site		
	Tsen-Wen seawall	Chi-Gu seawall[a]	Mi-Tou seawall
Average slope of the seabed (tan θ)	1: 69	1: 84	1: 72
tan α_1(S1)	1: 1.5	1: 6.2	1: 2.0
EL_1	5.00 m	3.80 m	5.00 m
γ_{r1}	1.00	1.00	1.00
tan α_2(S2)	1: 6.0	1: 7.0	1: 7.0
EL_2	2.00 m	1.30 m	2.32 m
γ_{r2}	0.55	0.55	0.55
tan α_3(S3)		1: 7.0	
EL_3		1.00 m	
γ_{r3}		0.55	

(tan α: slope; EL: crest elevation; γ_r: influence factor for roughness; subscripts 1, 2, and 3, indicate the seawall, revetment, and tetrapod section; respectively.).

[a] Note that on the front side of the Chi-Gu seawall, tetrapod was added to dissipate the wave energy. The associated parameters are also provided in this table.

instruments, including the conductivity controller, data logger, and general packet radio service (GPRS) module. Furthermore, the monitoring system was equipped with an independent power supply system composed of three solar panels and six storage batteries for the purpose of long-term monitoring. The GPRS module was used to transmit the collected data in real time to the Coastal Ocean Monitoring Center (COMC), National Cheng Kung University. The cables between the control station and the sensors were run through a flat iron pipe that was fixed onto the seawall.

In the early stages of this study in 2013–2014, the data logger (CR1000, Campbell Scientific, UT, USA) was used to acquire the signals of the conductivity sensors at a sampling rate of 1 Hz. Since 2015, the sampling rate was upgraded to 2 Hz by utilizing another data logger (BirdBox-A™, TERN, CA, USA). During the study period, the data logger continuously scanned and stored the voltage signals from the conductivity sensors. For each sensor, the hourly maximum signal could be identified from the signal data recorded over 1 h. The maximum voltage signals of all sensors were transmitted to COMC and compared with the threshold voltage (1.3 V) to confirm whether the sensors were submerged in seawater. The hourly maximum wave run-up height for the seawall could then be determined because the elevation of each sensor was known. Accordingly, the accuracy of the measured run-up height depended on the number of sensors deployed. The relationship between conductivity (c, unit: mS/cm) and voltage signal (V, unit: voltage) is expressed as Eq. (1), which was provided by the sensor manufacturer.

$$c = 62.5(V - 1) \tag{1}$$

According to Eq. (1), the threshold voltage 1.3 V corresponds to a conductivity value of 18.75 mS/cm (18,750 $\mu S/cm$, 12 ppt), which is equivalent to approximately 12 g of salt per kg of seawater.

To test the capability of the developed wave run-up monitoring system, the system was deployed on three seawalls in the southwestern coast of Taiwan, namely the Tsen-Wen, Chi-Gu, and Mi-Tou seawalls. The first two seawalls are in the Chi-Gu district of Tainan City, and the third seawall is in the Mi-Tou district of Kaohsiung City. As evident in Fig. 1 (b), on the front side of the Chi-Gu seawall, additional tetrapod was installed to dissipate wave energy. Fig. 2 (a) depicts a map of the island of Taiwan and the locations of Chi-Gu district, Tainan City, and Mi-Tou district, Kaohsiung City. Fig. 2 (b) and (c) depict the locations of the three seawalls.

Table 1 lists the values of the parameters in the empirical formulas for determining the wave run-up height. These parameters include the average slope of the seabed near a seawall (tan θ), slope (tan α), crest

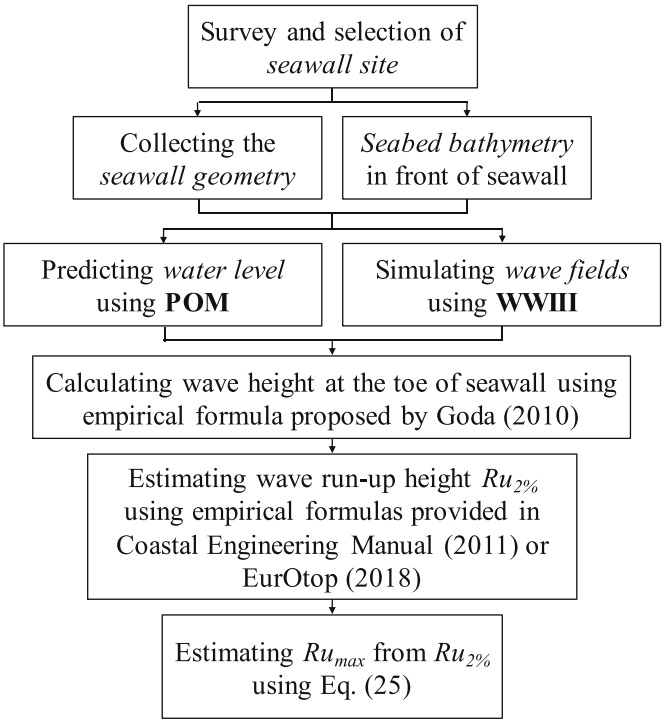

Fig. 3. Model for estimating the maximum wave run-up height $Ru_{\max}$ on a seawall.

elevation (EL), and roughness factor (γ_r) of the seawalls (subscript 1), revetment (subscript 2), and tetrapod (subscript 3). The wave run-up monitoring system was installed in the same manner on each seawall. Because the length of the seaward slope was different for each seawall, to obtain superior resolution of the run-up height, the longer slope was equipped with a greater number of conductivity sensors. Five sensors were installed on the Tsen-Wen seawall at elevations of 4.45 m, 3.90 m, 3.35 m, 2.80 m, and 2.25 m above the mean sea level (AMSL); six sensors were installed on the Chi-Gu seawall at elevations of 3.80 m, 3.30 m, 2.80, 2.30 m, 1.80 m, and 1.30 m AMSL; and seven sensors were installed on the Mi-Tou seawall at elevations of 5.00 m, 4.55 m, 4.11 m, 3.66 m, 3.21 m, 2.77 m, and 2.32 m AMSL. Notably, the vertical resolution of run-up measurements is approximately 0.5 m, which may not suffice for accurately measuring the run-up height. The accuracy could have been improved by installing more sensors; however, in the real application of wave run-up monitoring the main concern may not be accuracy but rather the approximate elevation difference between the maximum run-up level and the seawall crest.

3. Operational forecasting of wave run-up on the seawall

In this study, the authors additionally developed a model for operational forecasting of the maximum wave run-up height on seawalls; this model is illustrated in Fig. 3. Notably, as evident in Fig. 3, after gathering data about seawall geometry and seabed bathymetry in front of the seawall, the POM and WWIII model were used to predict the water levels and ocean waves, respectively. Goda's empirical formula (Goda, 2010) was then applied to determine the wave transformation from the offshore to the toe of the seawall. Subsequently, empirical formulas provided in the Coastal Engineering Manual (2011), for brevity hereafter CEM (2011), and EurOtop (2018) were used to estimate the wave run-up height. Finally, a method was proposed to estimate the ratio of the maximum run-up height $Ru_{\max}$ to the run-up height exceeded by 2% of the number of incident waves $Ru_{2\%}$.

3.1. Prediction of water levels and ocean waves

In this study, the POM (Blumberg and Mellor, 1987) and the WWIII model (Komen et al., 1984; Tolman, 1991; Komen et al., 1994; The WAVEWATCH III Development Group, 2016) were used to generate 72-h forecasts of hourly water levels and ocean waves, respectively, from the forecasted wind fields. The Central Weather Bureau (CWB), Taiwan, used the Weather Research and Forecasting (WRF) model (Hsiao et al., 2012; Power et al., 2017) to provide 72-h forecasts of hourly wind fields, renewed at 6-h intervals.

The POM was run on a finite element grid system to provide the water levels. The length of the linear triangular element grid was approximately 20 km in the offshore region and approximately 1.5 km in the nearshore region. The WWIII model provides the significant wave height (H_S) and mean wave period (T_m) and was run on a Cartesian grid system with a grid resolution of 0.25° (approximately 27.5 km). The water surface elevation within each gird cell, as obtained using the POM, was assumed to be constant. However, variations in the significant wave height from the offshore to the nearshore needed to be resolved because the grid size was considerably larger than the local wave length.

3.2. Wave transformation from the offshore to the toe of the seawall

Wave transformation, which usually involves shoaling, refraction, and wave breaking and occurs from offshore to shallow water, is a complex process. Although numerical models that solve the shallow water equations, Boussinesq equations, or Navier-Stokes equations can be used to determine the wave fields from the offshore area to the nearshore area, for simplicity, this study uses the empirical formula proposed by Goda (2010) to estimate the significant wave height from the deep water area to the toe of the seawall. Goda (2010) stated that for most practical applications, the wave height within the surf zone can be estimated by the following formula. This formula was obtained after regression analysis of laboratory and field survey data obtained at Sakata Harbor, Japan.

$$H_S = \begin{cases} K_S \cdot H_o & h/L_o \geq 0.2 \\ \min(\beta_o H_o + \beta_1 h,\ \ \beta_{\max} H_o,\ \ K_S \cdot H_o) & h/L_o < 0.2 \end{cases} \tag{2}$$

where H_S denotes the significant wave height at the local water depth h, K_S the shoaling coefficient, and H_o and L_o the wave height and wave length in deep waters, respectively. The parameters in Eq. (2) are defined as follows:

$$K_S = \sqrt{\frac{(C_g)_o}{C_g}} = \left[\left(1 + \frac{2kh}{\sinh 2\,kh}\right)\tanh kh\right]^{-\frac{1}{2}} \tag{3}$$

$$\beta_o = 0.028\ \ (H_o/L_o)^{-0.38}\ \exp\left(20\tan^{1.5}\theta\right) \tag{4}$$

$$\beta_1 = 0.52\ \ \exp(4.2\tan\theta) \tag{5}$$

$$\beta_{\max} = \max\left[0.92\ \ ,\ \ \ 0.32\ \ (H_o/L_o)^{-0.29}\ \exp(2.4\tan\theta)\right] \tag{6}$$

where C_g denotes the wave group velocity, subscript "o" the deep water condition, k the wavenumber, and $\tan\theta$ the bed slope near the toe of the seawall. Notably, the application of Goda's formula was divided into deep sea ($h/L_o \geq 0.2$) and shallow waters ($h/L_o < 0.2$). Once the water level and significant wave height at the toe of the seawall were determined, available empirical formulas were used to forecast the wave run-up height over the subsequent three days.

3.3. Empirical formulas for estimating wave run-up height

To determine the wave run-up height on the seawall, several empirical formulas have been proposed; for example, those provided in the CEM (2011), EurOtop (2018), and TAW (2002). These empirical

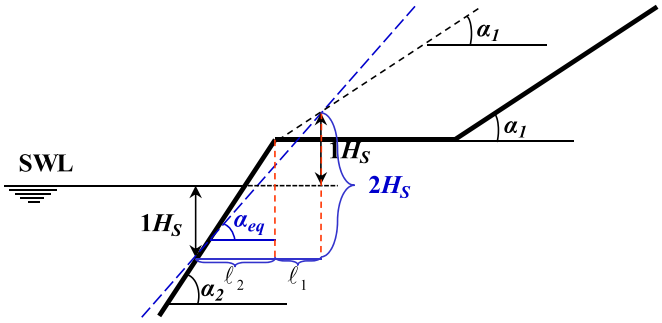

Fig. 4. Definition of an equivalent slope, $\tan\alpha_{eq}$, for seawall without berm (De Waal and Van der Meer, 1992).

formulas were established based on a series of laboratory experiments and field tests conducted on various types of seawalls. In this study, we adopted the empirical formulas recommended in the CEM (2011) and EurOtop (2018) to determine the wave run-up height on the three seawalls. The recommended empirical formulas from both manuals are given and discussed briefly as follows.

As mentioned in the Introduction, Van der Meer and Stam (1992) conducted experiments of irregular wave run-up on the slope of a seawall. The wave run-up thus obtained was characterized by a dimensionless surf similarity parameter called the Iribarren number. Accordingly, the run-up height can be expressed as follows.

$$\frac{Ru_{2\%}}{H_S} = 1.5\cdot\xi_p \text{ with a maximum value of } 3.0 \tag{7}$$

where $Ru_{2\%}$ denotes the level with respect to still water level (SWL), which is exceeded by 2% of the number of incident waves. According to the recommendations in TAW (2002), the significant wave height at the toe of the seawall can be set as the incident wave condition. The variable ξ_p denotes the Iribarren number, which is defined as:

$$\xi_p = \frac{\tan\alpha}{\sqrt{s_p}} \tag{8}$$

where $\tan\alpha$ is the seawall slope, and s_p is the wave steepness, defined as:

$$s_p = \frac{H_S}{L_o} = \frac{2\pi}{g}\frac{H_S}{T_p^2} \tag{9}$$

where H_S denotes the significant wave height at the toe of the seawall, L_o the wavelength in deep water, and g the gravitational acceleration. T_p is the peak wave period, and it is often used to determine s_p instead of the mean wave period (T_m).

Van der Meer and Stam (1992) prescribed the range of $T_p/\ T_m = 1.1 - 1.2$. In the present study, T_m was obtained using the WWIII model. It remained unchanged during the wave propagation from the deep water to the shallow water, and $T_p/T_m = 1.1$was adopted because both TAW (2002) and EurOtop (2018) recommended this value. Mazaheri and Ghaderi (2011) analyzed wave data recorded at different water depths (2.5–22 m) and proposed that $T_p/T_m \cong 1.5$. However, the displayed T_p and T_m data are widely scattered around the proposed regression line. Valid values of T_p/T_m in the shallow water area and their effects on the wave run-up height require further investigation.

3.3.1. *Empirical formulas from CEM (2011)*

By analyzing a large set of experimental data, De Waal and Van der Meer (1992) suggested empirical formulas for estimating the wave run-up height and mean overtopping discharge on the slope of a seawall under a wide range of wave conditions. These formulas have been included in the CEM (2011). Equation (10) presents the wave run-up height, $Ru_{2\%}$, in terms of the parameters associated with the geometry of the seawall, roughness, berm, shallow water, and oblique wave attack.

$$\frac{Ru_{2\%}}{H_S} = \begin{cases} 1.5\cdot\xi_{eq}\cdot\gamma_r\cdot\gamma_b\cdot\gamma_h\cdot\gamma_\beta & for\ \ 0.5 < \xi_{eq} < 2 \\ 3.0\cdot\gamma_r\cdot\gamma_b\cdot\gamma_h\cdot\gamma_\beta & for\ \ \xi_{eq} \geq 2 \end{cases} \tag{10}$$

where ξ_{eq} denotes the dimensionless surf similarity parameter based on an equivalent slope, γ_r the influence factor for roughness of the slope, γ_b the influence factor for a berm, γ_h the influence factor for a shallow foreshore, and γ_β the influence factor for oblique wave attack.

To account for seawall roughness, the following empirical formula for γ_r was suggested in TAW (2002).

$$\gamma_r = \frac{\sum_i \gamma_i L_i}{\sum_i L_i} \tag{11}$$

where γ_i denotes the influence factor for the i-th rough section of the slope, and L_i denotes the length of the i-th rough section. A seawall without a berm, $\gamma_b = 1.0$.

If a seawall does not have a berm and the seaward slope comprises two sections having different slopes, De Waal and Van der Meer (1992) suggested that the equivalent slope can be determined as follows; refer to Fig. 4.

$$\tan\alpha_{eq} = 2H_S/(\ell_1 + \ell_2) \tag{12}$$

where

$$\ell_1 = [H_S - (\mathrm{EL}_2 - SWL)]\cdot\mathrm{cotan}\,(\alpha_1) \tag{13a}$$

and

$$\ell_2 = [H_S + (\mathrm{EL}_2 - SWL)]\cdot\mathrm{cotan}\,(\alpha_2) \tag{13b}$$

The dimensionless surf similarity parameter based on the equivalent slope can then be defined as follows:

$$\xi_{eq} = \frac{\tan\alpha_{eq}}{\sqrt{s_p}} \tag{14}$$

De Waal and Van der Meer (1992) indicated that when a shallow foreshore is present in front of the seawall, the higher waves will break before they reach the seawall. For a gentle foreshore slope of 1:100, based on the experimental data they provide the following formula for γ_h:

$$\gamma_h = \begin{cases} 1 - \ 0.03(4 - h/H_S)^2 & for\ \ 1 \leq h/H_S \leq 4 \\ 1 & for\ \ h/H_S \geq 4 \end{cases} \tag{15}$$

where h and H_S denotes the water depth and significant wave height at the toe of the seawall. As shown in Table 1, the average slope of the seabed in front of the studied seawalls is mild and ranges from 1:69 to 1:84. Accordingly, Eq. (15) was adopted in this study to determine the influence factor for the shallow foreshore γ_h.

The coastlines of southwestern Taiwan have an almost straight and parallel bathymetric contour. According to Snell's law, the incident waves tend to approach the seawall normally. Therefore, in this study, the waves incident to the seawall are assumed to be normal, and $\gamma_\beta = 1$.

Notably, to apply Eq. (10) for estimating the wave run-up height, ξ_{eq} and four parameters, namely γ_r, γ_b, γ_h, and γ_β, must be given. In this study, for the Tsen-Wen and Mi-Tou seawalls, the seaward slope comprised two sections. If the SWL plus the significant wave height ($SWL + 1.0H_S$) exceeded the elevation of the revetment (EL_2), Eq. (12) was applied to determine the equivalent slope ($\tan\alpha_{eq}$). Otherwise, $\tan\alpha_{eq} = \tan\alpha_2$. For the Chi-Gu seawall, the section with tetrapod was considered a separate section with its own slope ($\tan\alpha_3$), elevation (EL_3), and roughness (γ_{r3}). Similarly, if $SWL + 1.0H_S \geq EL_2$, then Eq. (12) was used to determine $\tan\alpha_{eq}$. However, if $EL_3 \leq SWL + 1.0H_S < EL_2$, then α_2 and α_3 were used to determine $\tan\alpha_{eq}$ with Eq. (12). Finally, when $SWL + 1.0H_S < EL_3$, $\tan\alpha_{eq} = \tan\alpha_3$.

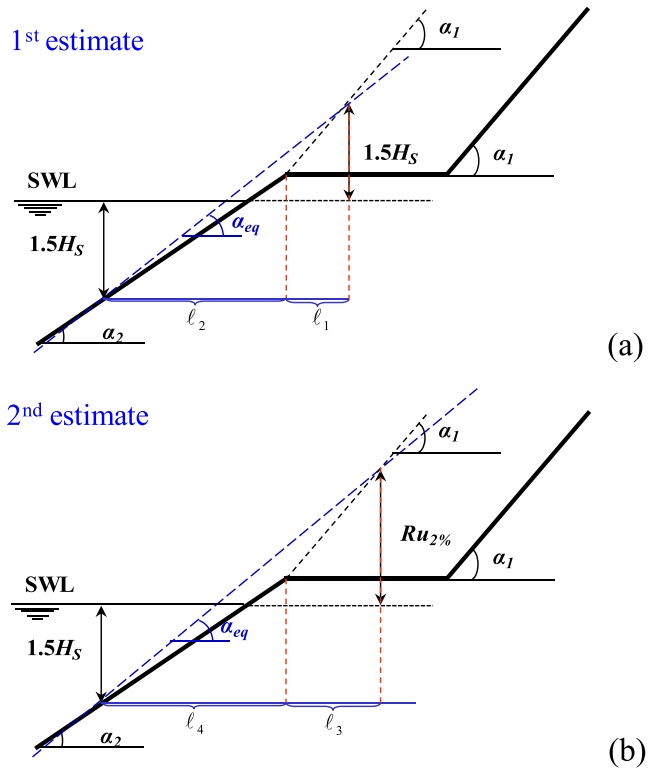

Fig. 5. Definition of an equivalent slope, $\tan\alpha_{eq}$, in EurOtop (2018); (a) first estimate of $\tan\alpha_{eq}$ and (b) second estimate of $\tan\alpha_{eq}$.

Table 2
Information about the typhoons that induced wave run-up on the studied seawalls.[a]

Case	Site	Typhoon (Scale)	Maximum wind speed (m/s)	Storm radius at wind scale 7[b] (km)	Date when typhoon was near Taiwan
1	Tsen-Wen seawall	**Trami** (mild)	30	180	Aug. 21, 2013
		Usagi (strong)	55	280	Sep. 21, 2013
2	Chi-Gu seawall Mi-Tou seawall	**Soudelor** (moderate)	48	300	Aug. 7–8, 2015
3	Chi-Gu seawall	**Meranti** (strong)	60	220	Sep. 13–14, 2016
		Malakas (moderate)	45	180	Sep. 16–17, 2016

[a] Data source: https://www.cwb.gov.tw.
[b] Wind scale 7 corresponds to a wind speed range of 13.9–17.1 m/s based on the Beaufort scale.

The shallow foreshore factor γ_h can be determined easily using Eq. (15), and as mentioned earlier, for a seawall without a berm, $\gamma_b = 1.0$, and for simplicity, $\gamma_\beta = 1.00$. EurOtop (2018) suggests the following values for the roughness factor of various armor layers: for a smooth impermeable surface, $\gamma_r = 1.00$, and for a revetment comprising two rock layers with an impermeable core, $\gamma_r = 0.55$. These values were adopted in this study, as summarized in Table 1. In addition, EurOtop (2018) provides the value of γ_r for the tetrapod section. However, the shape of the tetrapod used in this study differed from the shape used in EurOtop (2018). Accordingly, the roughness factor of the tetrapod, as summarized in Table 1, was calibrated through a comparison of the forecasted and measured run-up heights. After the roughness factors of various sections of the slope were determined, Eq. (11) was used to compute the representative roughness to be used in Eq. (10).

3.3.2. *Empirical formulas from EurOtop (2018)*

Similar to Eq. (10) provided in the CEM (2011), formulas provided by EurOtop (2018) can be used to estimate $Ru_{2\%}$ for gentle slopes. The formulas are written as follows:

$$\frac{Ru_{2\%}}{H_S} = \begin{cases} 1.65\cdot\gamma_b\cdot\gamma_r\cdot\gamma_\beta\cdot\xi_{eq} & for\ \ 0.5 < \xi_{eq} \le 1.8 \\ 1.0\cdot\gamma_r\cdot\gamma_\beta\left(4 - \dfrac{1.5}{\sqrt{\gamma_b\cdot\xi_{eq}}}\right) & for\ \ \xi_{eq} > 1.8 \end{cases} \quad (16)$$

The parameters of Eq. (16) are nearly the same as those in Eq. (10), except that the influence factor of a shallow foreshore γ_h is not considered by the EurOtop (2018) formulas, and the EurOtop definition of the equivalent slope $\tan\alpha_{eq}$ is different from that in the CEM (2011). In the EurOtop (2018) formulas, the equivalent slope is determined using two steps. In the first step, $\tan\alpha_{eq}$ is estimated as follows (refer to Fig. 5 (a)):

$$\tan\alpha_{eq} = 3H_S/(\ell_1 + \ell_2) \quad (17)$$

where

$$\ell_1 = [1.5H_S - (EL_2 - SWL)]\cdot\cot(\alpha_1) \quad (18a)$$

and

$$\ell_2 = [1.5H_S + (EL_2 - SWL)]\cdot\cot(\alpha_2) \quad (18b)$$

The $\tan\alpha_{eq}$ obtained from Eq. (17) is used to determine ξ_{eq} by Eq. (14) and to estimate $Ru_{2\%}$ by Eq. (16). After the first estimate of $Ru_{2\%}$ is obtained, its value is used to derive the second estimate of $\tan\alpha_{eq}$ as follows (refer to Fig. 5 (b)):

$$\tan\alpha_{eq} = [1.5H_S + Ru_{2\%}(first\ \ estimate)]/(\ell_3 + \ell_4) \quad (19)$$

where

$$\ell_3 = [Ru_{2\%} - (EL_2 - SWL)]\cdot\cot(\alpha_1) \quad (20a)$$

and

$$\ell_4 = [1.5H_S + (EL_2 - SWL)]\cdot\cot(\alpha_2) \quad (20b)$$

The second estimate of $\tan\alpha_{eq}$ is used to determine ξ_{eq} by Eq. (14) and then to estimate $Ru_{2\%}$ by Eq. (16).

When Eq. (16) is used to estimate the run-up height, the method used to determine the equivalent slopes of various seawalls under various incident wave conditions is similar to that used when Eq. (10) is applied. The seaward slope of the Tsen-Wen and Mi-Tou seawalls comprises two sections. Therefore, if $SWL + 1.5H_S < EL_2$, then $\tan\alpha_{eq} = \tan\alpha_2$. If $SWL + 1.5H_S \ge EL_2$, then Eq. (19) is applied to determine $\tan\alpha_{eq}$. For the Chi-Gu seawall, if $SWL + 1.5H_S < EL_3$, then $\tan\alpha_{eq} = \tan\alpha_3$. Moreover, if $EL_3 \le SWL + 1.5H_S < EL_2$, then α_2 and α_3 are used to determine $\tan\alpha_{eq}$ with Eq. (19). Furthermore, if $SWL + 1.5H_S \ge EL_2$, then Eq. (19) is used to determine $\tan\alpha_{eq}$.

Bathymetric information and seawall geometry are required for estimating the wave run-up height and overtopping discharge. Because the three studied seawalls are in the region administered by the Sixth River Management Office, Water Resources Agency (WRA), Taiwan, the relevant data were obtained from this office.

3.4. *Estimation of the ratio of Ru_{max} to $Ru_{2\%}$*

For simplicity, the operational wave run-up monitoring system measured the hourly maximum run-up height, Ru_{max}. However, the available empirical formulas for determining run-up height provide a value that is exceeded by 2% of the number of incident waves, $Ru_{2\%}$. In this study, the following method was applied to estimate the ratio of Ru_{max} to $Ru_{2\%}$.

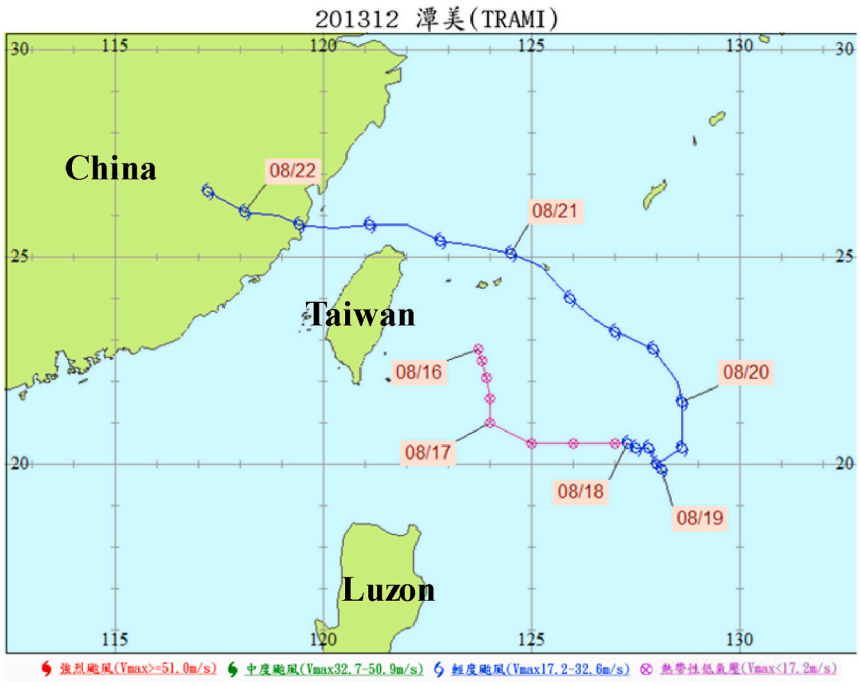

Fig. 6. (a) Path of typhoon Trami that passed over the north waters of Taiwan on August 21, 2013; (b) path of typhoon Usagi that passed over the south waters of Taiwan on September 21, 2013
(Data source: https://www.cwb.gov.tw)..

Assuming that the wave run-up height has a Rayleigh distribution similar to the wave height distribution (Saville, 1962; Battjes, 1971, 1974; Ahrens, 1977), then the wave height and wave run-up distribution are given as follows (Shore Protection Manual, 1984):

$$\frac{H_p}{H_S}=\frac{Ru_p}{Ru_S}=\left(-\frac{\ln p}{2}\right)^{1/2} \tag{21}$$

where H_p and Ru_p are the wave height and wave run-up height associated with a particular possibility of exceedance p and Ru_S is the wave run-up height of the significant wave height H_S.

Goda (2010) indicated that if the wave height has a Rayleigh distribution, then the most probable value for the ratio of the maximum wave height H_{max} to H_S is

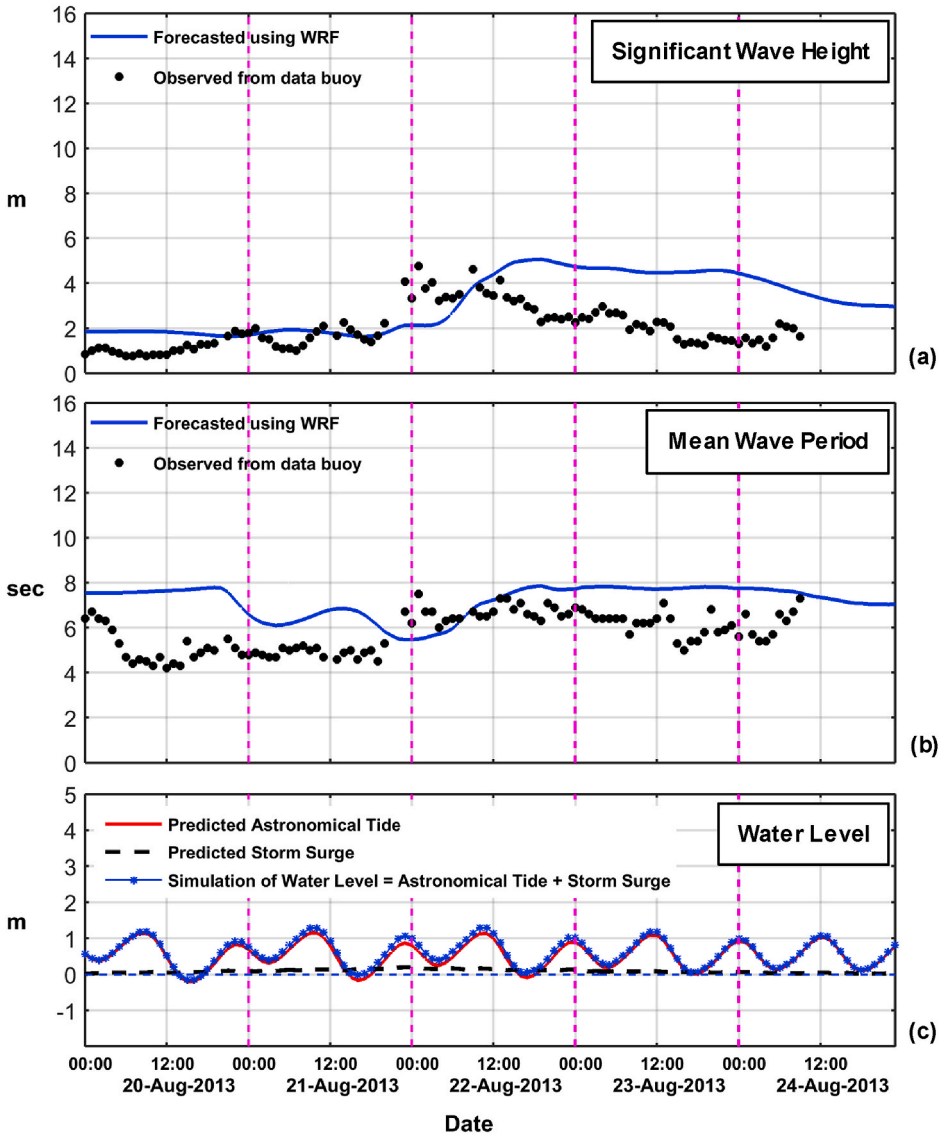

Fig. 7. Comparison of prdicted and measured offshore waves at the Chi-Gu buoy during typhoon Trami in terms of (a) significant wave height H_S and (b) mean wave period T_m. (c) Water levels at the buoy site predicted using POM.

$$\frac{H_{\max}}{H_S} \cong 0.706\sqrt{\ln N_o} \tag{22}$$

where N_o refers to the number of waves. Because the wave run-up also has a Rayleigh distribution, accordingly

$$\frac{Ru_{\max}}{Ru_S} \cong 0.706\sqrt{\ln N_o} \tag{23}$$

Combining Eqs. (23) and (21) yields

$$\frac{Ru_{\max}}{Ru_p} \cong \frac{0.706\sqrt{\ln N_o}}{\left(-\frac{\ln p}{2}\right)^{1/2}} \tag{24}$$

When p is 2 %, Eq. (24) becomes

$$\frac{Ru_{\max}}{Ru_{2\,\%}} \cong \frac{0.706\sqrt{\ln N_o}}{\left[-\frac{\ln(0.02)}{2}\right]^{1/2}} = 0.505\ \sqrt{\ln N_o} \tag{25}$$

If the maximum run-up height was provided hourly, then $N_o = 3600(s)/T_m(s)$. As mentioned in Section 3.1, the hourly mean wave period, T_m, was obtained using the WWIII model. Equation (25) was used in this study to estimate $Ru_{\max}/Ru_{2\%}$. In the case, when $T_m = 10s$, then $N_o = 360$, and $Ru_{\max}/Ru_{2\%} = 1.22$.

4. Results and discussion

The real-time wave run-up monitoring system described in Section 2 and the run-up forecasting model described in Section 3 were combined for the operational monitoring and forecasting of wave run-up on real seawalls. In 2013, 2014, the run-up monitoring system was installed on the Tsen-Wen seawall to evaluate the capabilities of the wave run-up forecasting system. Since 2015, the monitoring system has been deployed on Chi-Gu and Mi-Tou seawalls. The monitoring system was set up at the beginning of the typhoon season, which is usually in July, and retrieved at the end of the typhoon season, which is usually in October. Because seawalls in Taiwan are built tall, wave overtopping rarely occurs, even during typhoon periods. Since the monitoring system was set up in 2013, overtopping at the studied seawalls has been minor or undetected. Accordingly, this section presents only a comparison of wave run-up heights obtained from the real-time monitoring system with those obtained from operational forecasting. On average, three to four typhoons hit Taiwan annually, and only a few representative

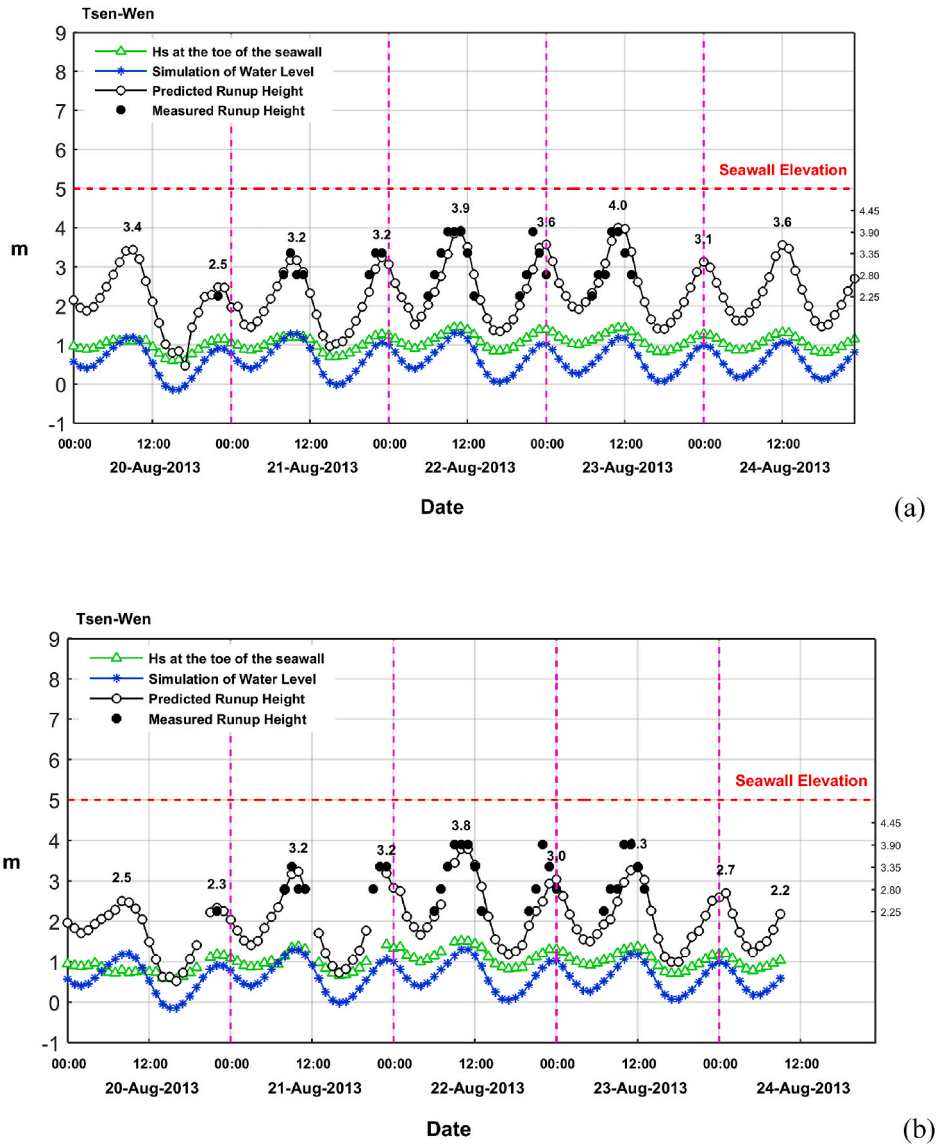

Fig. 8. Comparison of forecasted and measured hourly maximum wave run-up heights Ru_{max} on the Tsen-Wen seawall during typhoon Trami. The forecasted Ru_{max} was determined from $Ru_{2\%}$ estimated using Eq. (10). Offshore waves in (a) were predicted at a location in front of the seawall at a distance of approximately 3 km, whereas those in (b) were measured at the Chi-Gu buoy. The marked numbers on the right vertical axis of the lower figure denote the elevations of run-up sensors.

typhoon events were investigated in this study. Information about typhoons that induced wave run-up on the studied seawalls is summarized in Table 2. The table lists the typhoon scale, observed maximum wind speed, storm radius with a wind scale of 7, date on which the typhoon was near the island of Taiwan, and seawalls where run-up was investigated. A wind scale of 7 corresponds to a wind speed range of 13.9–17.1 m/s based on the Beaufort scale. Data summarized in Table 2 were obtained from the Taiwan CWB website (www.cwb.gov.tw). We did not investigate the wave run-up at studied seawalls in 2017 or 2018 because no large typhoons hit Taiwan and no significant wave run-up was observed during those years.

4.1. Run-up heights on the Tsen-Wen seawall during typhoons Trami and Usagi in 2013

The forecasted and measured hourly maximum wave run-up heights on the Tsen-Wen seawall were obtained during typhoons Trami and Usagi in 2013. As summarized in Table 2, typhoon Trami was a mild typhoon, and typhoon Usagi was a strong typhoon. Fig. 6 (a) and (b) illustrate the tracks of typhoons Trami and Usagi, respectively. Typhoon Trami passed over the waters north of Taiwan on August 21, 2013, and typhoon Usagi passed over the waters south of Taiwan on September 21, 2013. Although neither typhoon passed through the island of Taiwan, swells induced by the two typhoons greatly affected the southwestern coast of Taiwan such that wave run-up was observed on the Tsen-Wen seawall.

As stated in Section 3, after forecasted wind fields obtained using the WRF model were provided by the CWB, POM was applied to obtain the water level, which involved the astronomical tide and storm surge, and the WWIII model was used to predict the significant wave height (H_S) and mean wave period (T_m) in the offshore region. To demonstrate how the WWIII model predicts offshore waves, Fig. 7 (a) compares the predicted and measured H_S at the Chi-Gu buoy during typhoon Trami, and the corresponding comparison for T_m is presented in Fig. 7 (b). The Chi-Gu buoy was located approximately 3.4 km away from the northwestern side of the Tsen-Wen seawall (Fig. 2). The measured H_S and T_m values terminate at 09:00 on August 24, 2013, because at this time, the mooring line of the buoy was broken, and the buoy drifted away. Detailed information on the Chi-Gu buoy is provided in Section 4.2. Fig. 7 (c) presents the POM-predicted water level during the same

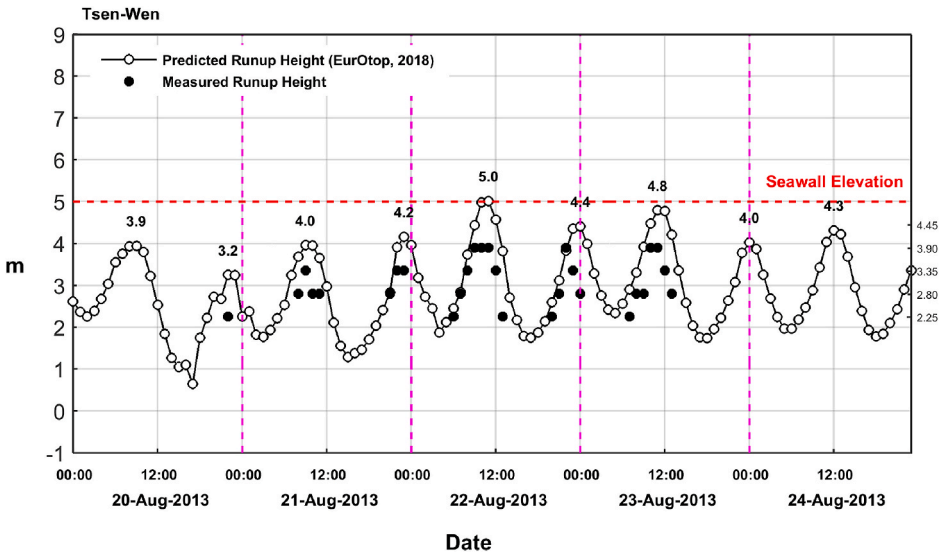

Fig. 9. Comparison of forecasted and measured hourly maximum wave run-up heights Ru_{max} on the Tsen-Wen seawall during typhoon Trami. The forecasted Ru_{max} was determined from $Ru_{2\%}$ estimated using Eq. (16). Offshore waves were predicted using the WWIII model. The marked numbers on the right vertical axis of the lower figure denote the elevations of run-up sensors.

Table 3
Information about the water depth and incident wave conditions at the toe of the seawall and some key parameters for estimating $Ru_{2\%}$ from 08:00 to 16:00 on August 22, 2013, on the Tsen-Wen seawall during typhoon Trami.

Site		Tsen-Wen seawall								
Parameter		Time								
		August 22, 2013								
		08:00	09:00	10:00	11:00	12:00	13:00	14:00	15:00	16:00
H (m)		1.954	2.132	2.279	2.281	2.132	1.876	1.519	1.239	1.062
WL(m)		0.966	1.144	1.291	1.293	1.144	0.888	0.531	0.251	0.074
$H_S(m)$		1.255	1.359	1.448	1.458	1.387	1.261	1.077	0.933	0.843
T_m(s)		6.43	6.60	6.84	7.01	7.17	7.39	7.52	7.57	7.60
h/H_S		1.557	1.569	1.574	1.564	1.537	1.488	1.410	1.328	1.260
CEM (2011)	γ_h	0.821	0.823	0.823	0.822	0.818	0.811	0.799	0.786	0.775
	$\tan\alpha_{eq}$	0.178	0.194	0.206	0.207	0.195	0.174	0.167	0.167	0.167
	ξ_{eq}	1.407	1.505	1.610	1.648	1.628	1.577	1.659	1.795	1.895
	Ru_{max}	2.758	3.318	3.848	3.915	3.503	2.808	2.143	1.675	1.372
EurOtop (2018)	$\tan\alpha_{eq}$	0.205	0.219	0.230	0.230	0.219	0.199	0.173	0.167	0.167
	ξ_{eq}	1.615	1.703	1.796	1.837	1.829	1.800	1.719	1.795	1.895
	Ru_{max}	3.737	4.432	4.979	5.014	4.569	3.818	2.786	2.167	1.783
	$\gamma_h Ru_{max}$	3.068	3.648	4.098	4.122	3.737	3.096	2.226	1.703	1.382

(h: the water depth at the toe of seawall, $h = h_o + WL$; h_o: the still water depth; WL: the water level due to the astronomical tide and storm surge; γ_h: the influence factor for a shallow foreshore).

typhoon period. Variations in astronomical tide and storm surge during the typhoon period are revealed. The comparison of predicted and measured H_S and T_m values in Fig. 7 (a) and (b) reveals that the WWIII model provided an approximate estimation of offshore waves.

Fig. 8 (a) and (b) present a comparison of the forecasted and measured hourly maximum wave run-up heights Ru_{max} on the Tsen-Wen seawall during typhoon Trami. The line with white circles represents forecasted run-up heights, and black dots represent measured values. As mentioned in Section 3.2, the coastlines of southwestern Taiwan have a nearly straight and parallel bathymetric contour; therefore, waves incident to the seawall are assumed to be normal. Accordingly, offshore waves used to determine the H_S at the toe of the seawall were provided by the WWIII model at a location approximately 3 km in front of the seawall. Offshore waves in Fig. 8 (a) were provided at this location, and those in Fig. 8 (b) were measured at the Chi-Gu buoy. In Fig. 8 (b), some hours had no forecasted Ru_{max} because at these times, the observed offshore wave data were discarded for not satisfying the data quality criteria set by COMC, which is responsible for manipulating this data buoy. In addition, the comparison of the forecasted and measured Ru_{max} terminated at 09:00 on August 24, 2013, because the buoy drifted away at this time. Since then, no measured offshore wave data have been available to determine Ru_{max}. The Ru_{max} values in Fig. 8 (a) and (b) were determined from $Ru_{2\%}$, which was estimated using Eq. (10). Furthermore, the simulated water level (blue line with stars) and the H_S at the toe of the seawall (green line with triangles) are displayed in Fig. 8. The horizontal red dashed line represents the crest level of the seawall (5.0 m), and the elevations of run-up sensors are depicted on the right hand side of the figure. In Fig. 8, Ru_{max} values obtained from either the predicted or measured offshore waves during typhoon Trami are concurrent with measured values, and wave overtopping did not occur. Compared with measured wave data, predicted ocean waves produced more accurate run-up heights. This difference may have occurred because

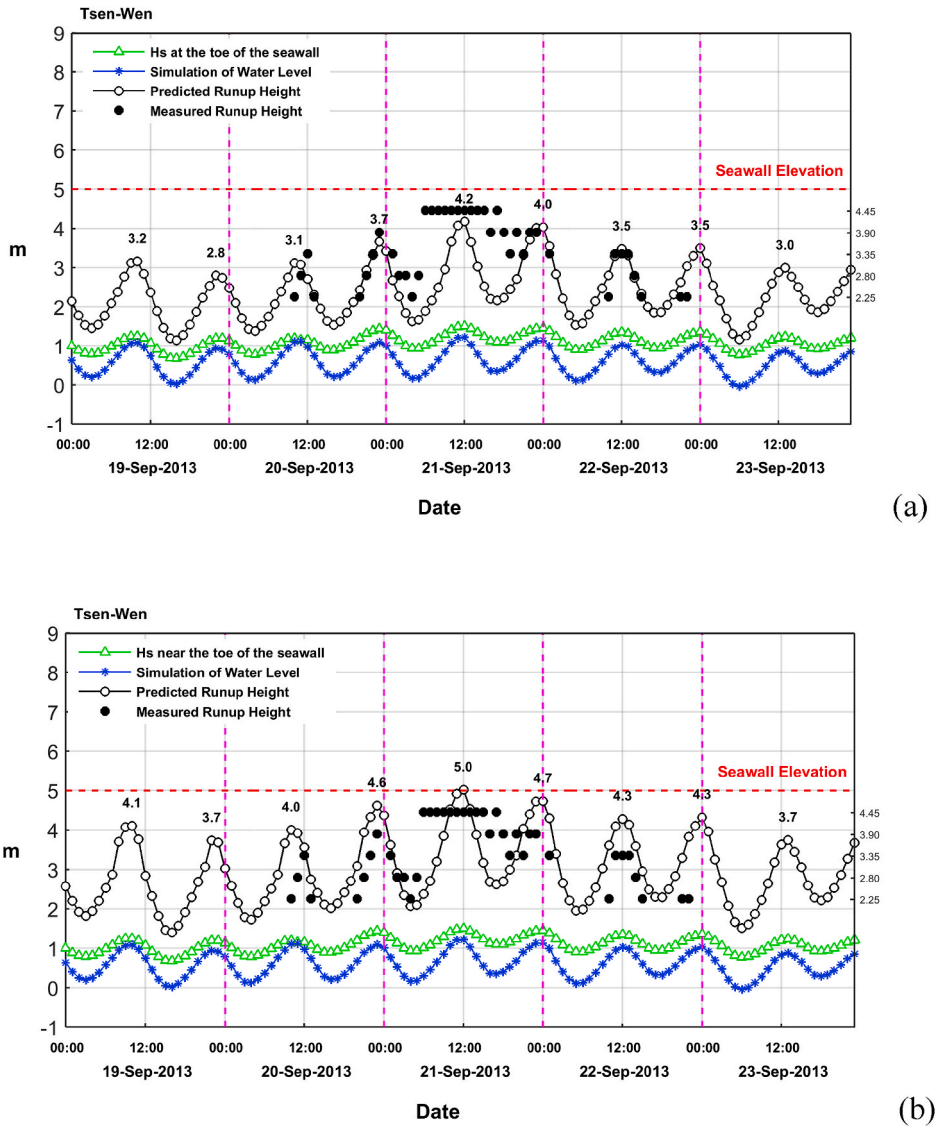

Fig. 10. Comparison of forecasted and measured hourly maximum wave run-up heights $Ru_{\max}$ on the Tsen-Wen seawall during typhoon Usagi; (a) $Ru_{2\%}$ was estimated using Eq. (10), and (b) $Ru_{2\%}$ was estimated using Eq. (16). The marked numbers on the right vertical axis of the lower figure denote the elevations of run-up sensors.

predicted ocean waves were provided at a more appropriate location relative to the seawall; therefore, predicted waves approximated more closely to the actual offshore waves to be used for determining the H_S at the toe of the seawall.

Similar to Figs. 8 (a), Fig. 9 presents a comparison of forecasted and measured hourly $Ru_{\max}$ values on the Tsen-Wen seawall during typhoon Trami. The forecasted $Ru_{\max}$ values in Fig. 9 were obtained from $Ru_{2\%}$, which was estimated using Eq. (16), as suggested by EurOtop (2018). Fig. 9 reveals that Eq. (16) overestimated the run-up height, but the overall trend was adequate. As mentioned before, parameters in Eq. (16) are basically the same as those in Eq. (10), except that in EurOtop (2018), the influence factor for a shallow foreshore γ_h is not considered, and the definition of $\tan\alpha_{eq}$ differs from that in the CEM (2011).

To explain why EurOtop (2018) formulas overestimated the run-up height on the Tsen-Wen seawall, detailed information on water depth and incident wave conditions at the toe of the seawall and some key parameters for estimating $Ru_{2\%}$ from 08:00 to 16:00 on August 22, 2013, are listed in Table 3. Notably from Table 3 that various definitions of $\tan\alpha_{eq}$ do not cause large differences in ξ_{eq} values. Therefore, influence factor for a shallow foreshore γ_h should cause large differences in $Ru_{\max}$ values.

De Waal and Van der Meer (1992) introduced γ_h to the run-up formula for the following reasons: As mentioned in Section 3.4, if the wave run-up height is assumed to have a Rayleigh distribution similar to the wave height, then Eq. (21) indicates that $\frac{Ru_{2\%}}{Ru_S} = \frac{H_{2\%}}{H_S}$, or $\frac{Ru_{2\%}}{H_S} = \frac{H_{2\%}}{H_S}\frac{Ru_S}{H_S} = 1.4\frac{Ru_S}{H_S}$. However, $\frac{H_{2\%}}{H_S} = 1.4$ is valid only when the wave height has Rayleigh distribution. When a shallow foreshore is present in front of a seawall, higher waves will break before they reach the structure. Therefore, the wave height at the toe of the structure no longer has a Rayleigh distribution. In these situations, $\frac{H_{2\%}}{H_S} = 1.4\,\gamma_h$. For a gentle foreshore slope of 1:100, De Waal and Van der Meer (1992) provided an empirical formula (Eq. (15)) for determining the values of γ_h. Accordingly,

$$\frac{Ru_{2\%}}{H_S} = 1.4\gamma_h\frac{Ru_S}{H_S} \tag{26}$$

This equation was further developed to have the form of Eq. (10). In Table 3, the values of h/H_S at the toe of the seawall range from 1.260 to 1.574 and γ_h values range from 0.775 to 0.823. If γ_h is also considered in run-up formulas provided by EurOtop (2018), then corrected $Ru_{\max}$

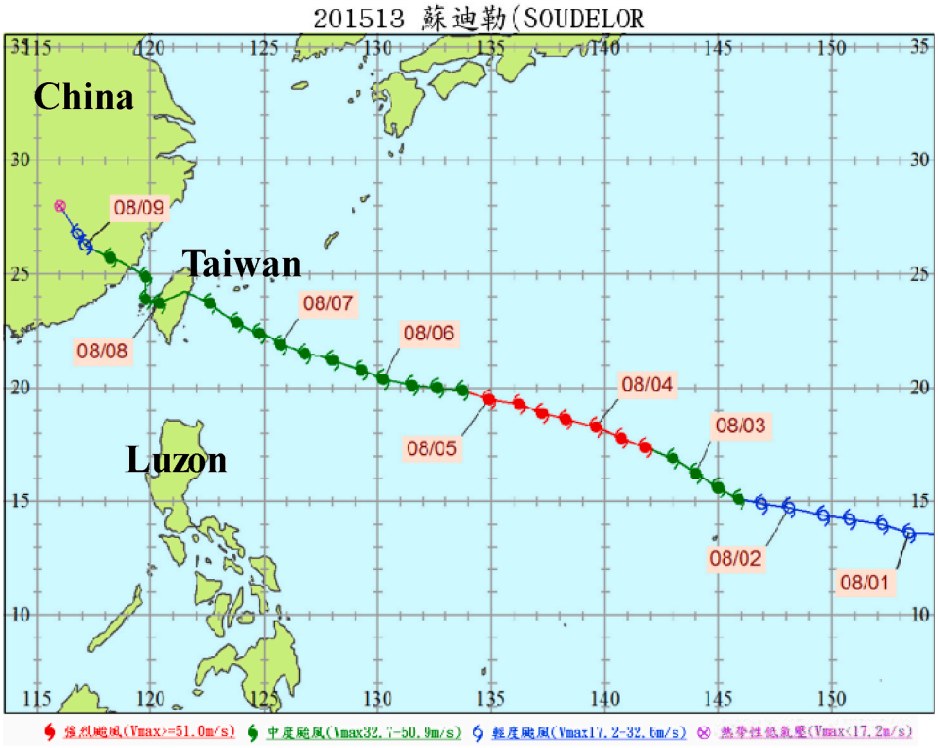

(Data source: https://www.cwb.gov.tw)

Fig. 11. Path of typhoon Soudelor that passed through the island of Taiwan on August 8, 2015 (Data source: https://www.cwb.gov.tw)..

values ($\gamma_h \cdot Ru_{max}$) are close to those obtained from formulas suggested in the CEM (2011). The data listed in Table 3 reveal that γ_h is the main factor causing considerable differences in Ru_{max}.

Similar to Fig. 8 (a) and 9, Fig. 10 (a) and (b) compare the measured Ru_{max} on the Tsen-Wen seawall during typhoon Usagi with the forecasted values obtained using various empirical formulas for $Ru_{2\%}$. The $Ru_{2\%}$ values in Fig. 10 (a) and (b) were estimated using Eqs. (10) and (16), respectively. The results presented in Fig. 10 (a) and (b) revealed that when H_S at the toe of the seawall was high, Eq. (16) overestimated run-up heights. A high H_S value implies a low h/H_S value. According to Eq. (15), when $1 \leq h/H_S \leq 4$, then $\gamma_h < 1.0$. Therefore, the inclusion of γ_h reduces the forecasted run-up height.

As evident in Eqs. (10) and (16), wave conditions at the toe of the seawall, including H_S, T_m, T_p, and wave direction, are crucial for estimating the run-up; accordingly, wave monitoring near or at the toe of the seawall, which was not performed in this study, is strongly recommended in future research. The measured wave conditions at the toe of the seawall can be used to evaluate whether H_S values at this location are correctly determined by the proposed methods. These H_S values can also be used to confirm the accuracy of empirical formulas for the run-up estimation, when measured run-up heights are available.

Because the H_S at the toe of the seawall is determined from offshore waves; accordingly, offshore wave data are crucial for accurately estimating run-up height. However, the accurate prediction of typhoon-induced ocean waves is difficult. Similar unsatisfactory run-up forecasting was encountered during typhoon periods in successive years. Accordingly, the multi-model ensemble approach (Pan et al., 2016) was introduced in 2015 to improve ocean wave prediction, and it eventually was used to present the forecasted run-up height as a band with upper and lower limits as opposed to a single value. The multi-model ensemble approach is discussed in Section 4.2.

4.2. Run-up heights on the Chi-Gu and Mi-Tou seawalls during typhoon Soudelor in 2015

Since 2015, wave run-up monitoring systems have been installed at the Chi-Gu seawall in Tainan City and the Mi-Tou seawall in Kaohsiung City. The locations of the two seawalls are indicated in Fig. 2. On August 8, 2015, the moderate-strength typhoon Soudelor passed through Taiwan. The coastal area where the typhoon moved away from the island is near Chi-Gu and Mi-Tou seawalls. Fig. 11 illustrates the path of typhoon Soudelor through the center of Taiwan on August 8, 2015.

In the early stages of this study, the POM and WWIII model were used to predict water levels and ocean waves, respectively, based on the wind fields forecasted using the WRF model. Therefore, only one predicted wave run-up height was available. However, making an accurate prediction of typhoon-induced ocean waves is a challenging task. Uncertainties arise from both the weather and hydrodynamic modeling systems due to the forcing conditions, modeling technique, and physical parameters. Recently, ensemble approaches have often been employed to reduce the uncertainties arising from the forcing conditions and physical parameters (Zou et al., 2013; Pan et al., 2016). In ocean wave modeling, ensemble approaches are usually classified into two types: parameter ensemble approach and model ensemble approach. In both approaches, a specific wave model is selected to produce wave fields by using various atmospheric forcing conditions. The parametric ensemble approach generates the ensemble members by using a weather model with perturbed physical parameters, and the model ensemble approach uses various weather models to generate the ensemble members for further statistical analysis to obtain the wave ensemble. Therefore, the model ensemble approach is occasionally called the multi-model ensemble approach. Similar to the multi-model ensemble approach of Pan et al. (2016), the approach adopted in the present study involved the use of wind fields obtained from three weather models since 2015 to generate three ocean waves as ensemble members. The three weather

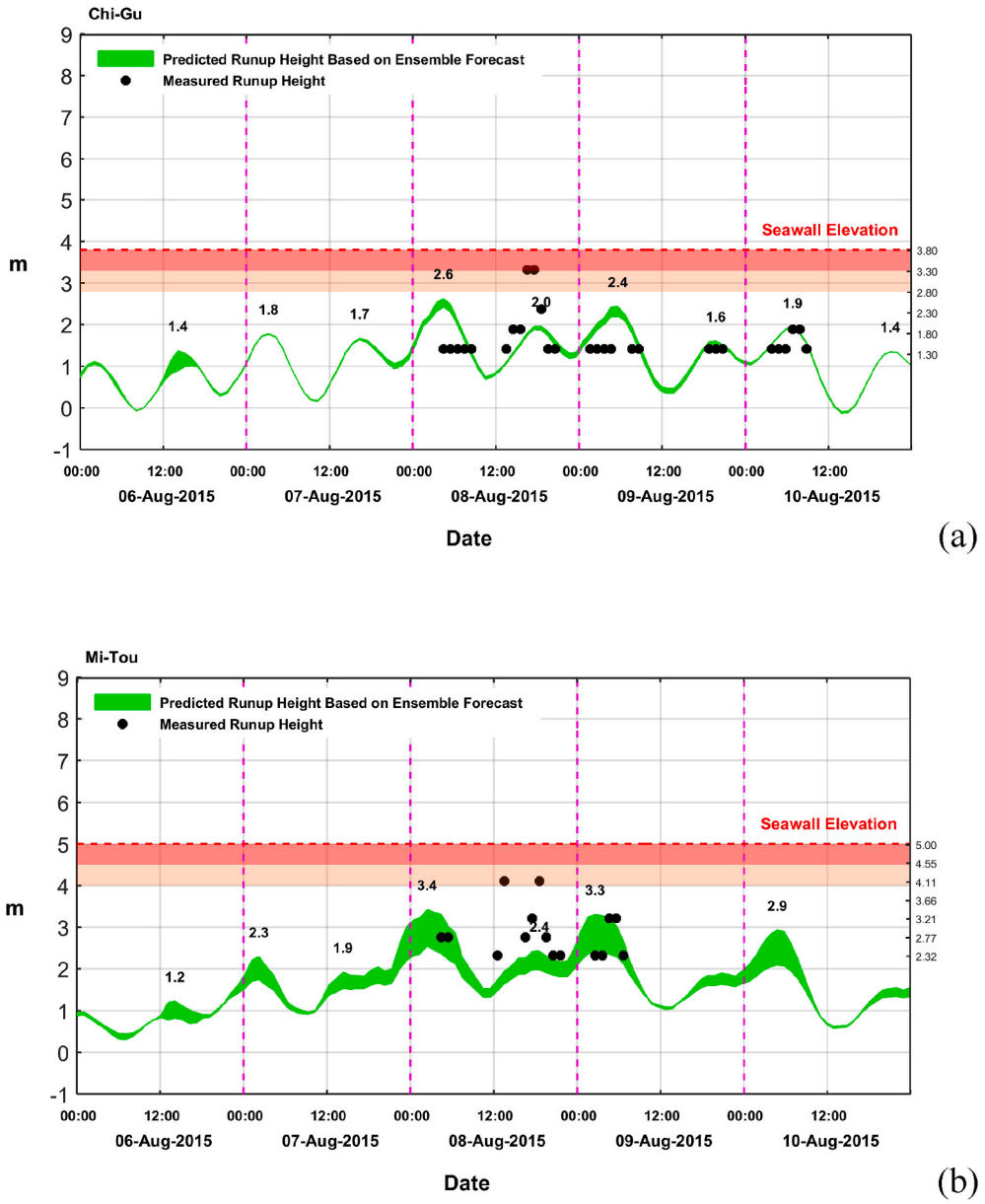

Fig. 12. Comparison of forecasted and measured hourly maximum wave run-up heights Ru_{max} at (a) the Chi-Gu seawall and (b) Mi-Tou seawall during typhoon Soudelor. The ocean waves simulated using three weather models, namely the NCEP, JMA, and WRF models, were used to determine the upper and lower limits of the possible wave run-up heights. The forecasted Ru_{max} was determined from $Ru_{2\%}$ estimated using Eq. (10).

models were the National Centers for Environmental Predictions (NCEP) model, Japan Meteorological Agency (JMA) model, and WRF model. Instead of using statistical analysis to produce the wave ensemble from the available members, in this study, the three ocean wave members were used to obtain the upper and lower limits of the possible wave run-up heights. Consequently, the forecasted maximum wave run-up height was no longer provided as a single value but instead as a band with a lower and an upper limit.

Fig. 12 (a) and (b) present the band of forecasted Ru_{max} values at Chi-Gu and Mi-Tou seawalls, respectively, during typhoon Soudelor. The forecasted Ru_{max} was determined from $Ru_{2\%}$, which was estimated using Eq. (10). The measured wave run-up heights at the two seawalls are included in the figures for comparison. The green band represents the ensemble forecast of wave run-up heights that was determined using the offshore wave conditions predicted by the wind fields obtained from the NCEP, JMA, and WRF models. Notably, Fig. 12 (a) and (b) indicate that from 05:00 on August 8 to 08:00 on August 9, the forecasted wave run-up heights on the Chi-Gu seawall were inconsistent with the measured values. The wave run-up heights on the Chi-Gu and Mi-Tou seawalls were considerably underestimated from 13:00 to 18:00 on August 8, 2015, when the typhoon was very close to the southwestern coast of Taiwan. Factors that significantly affect the estimation of wave run-up height are the bathymetry in front of the seawall, geometry of the seawall, and offshore wave conditions. In this study, the authors collected and annually updated the bathymetry information and the elevation data concerning the revetments and seawalls. A factor that possibly affects the accuracy of run-up forecast is then the offshore wave conditions.

As illustrated in Fig. 11, typhoon Soudelor passed through the middle of the island of Taiwan, which is a mountainous island, and more than 260 mountains on the island have peaks taller than 3,000 m; the height of the tallest peak Yushan is 3952 m high (http://www.mountaineering.org.tw). The mountain ranges are located mainly in the central part of Taiwan, and they stretch from north to south. As indicated by many

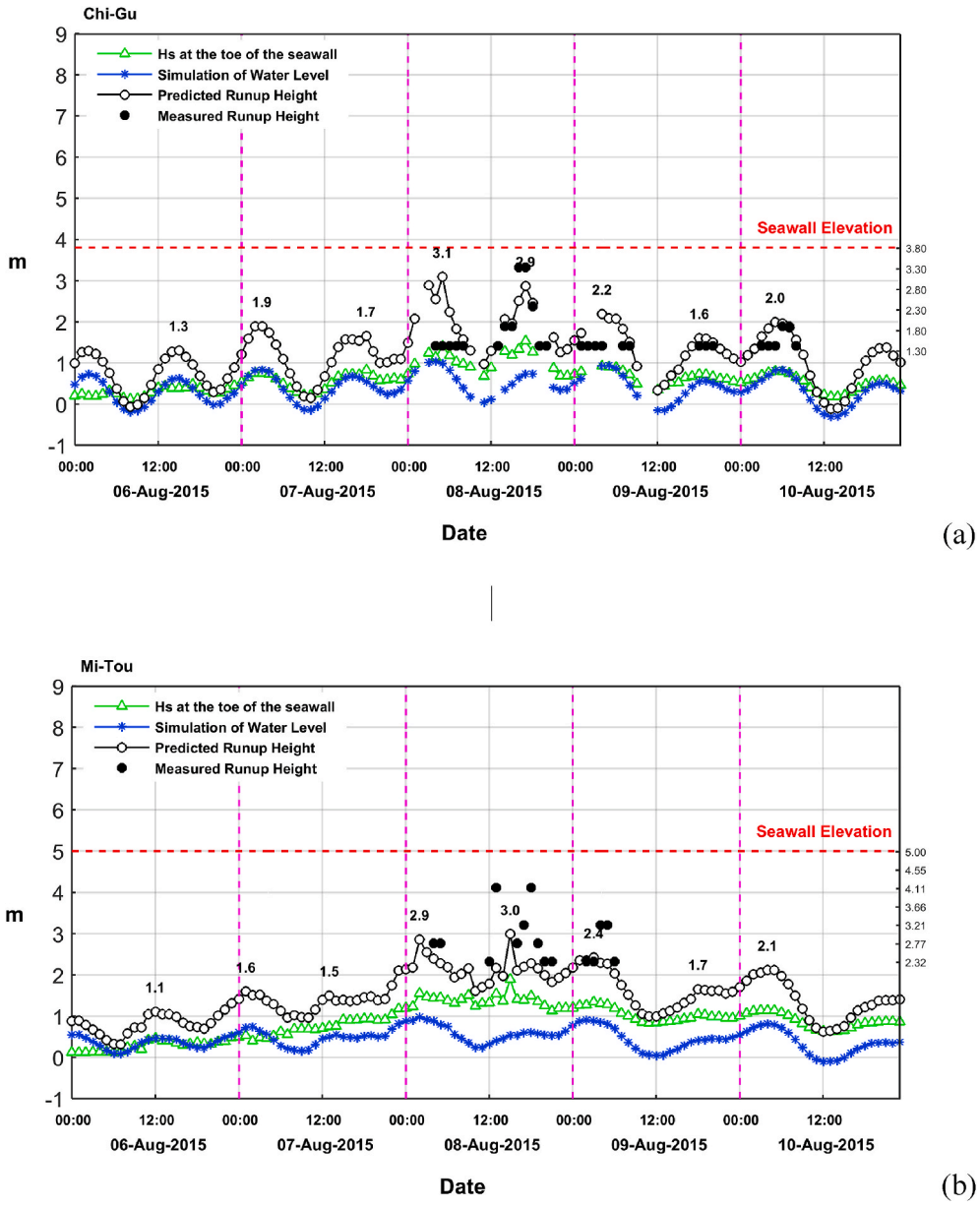

Fig. 13. Comparison of forecasted and measured hourly maximum wave run-up heights Ru_{max} at the (a) Chi-Gu seawall and (b) Mi-Tou seawall when measured wave data from nearby Chi-Gu and Mi-Tou data buoys were used as offshore wave conditions. The forecasted Ru_{max} was determined from $Ru_{2\%}$ estimated using Eq. (10).

researchers (Wu and Hong, 2007; Hsiao et al., 2012; Power et al., 2017), the forecasted wind values are affected not only by large-scale atmospheric conditions but also by topography. The topographic features of the island of Taiwan make it difficult to forecast the wind fields during typhoon periods, especially for typhoons that pass through the island from east to west, such as typhoon Soudelor. The topographic features may have been the main factors affecting the accurate simulation of the wind fields, which in turn led to inaccurate predictions of ocean waves and ultimately inaccurate run-up forecasting. However, topographic effects alone may not be sufficient for explaining why the forecast sometimes overestimated or underestimated the run-up height on the Chi-Gu seawall during the Soudelor typhoon period (Fig. 12 (a)). Reasons for this poor estimation and methods for improving the estimation of run-up height under storm conditions require further investigation.

The good agreement between the forecasted and measured wave run-up heights at the Tsen-Wen seawall, as illustrated in Fig. 8 (a) and 10 (a), during the periods of typhoons Trami and Usagi, respectively, may be ascribed to the fact that neither typhoon passed through the island. The topographic effects were minor. Accordingly, the forecasted wind fields were acceptable for obtaining accurate ocean waves. Moreover, although various wind models were adopted to obtain various ocean waves, for simplicity, the wind fields obtained with the WRF model were used in the POM to forecast water levels.

To further verify the accuracy and applicability of the proposed wave run-up forecasting system, observed wave data from nearby Chi-Gu and Mi-Tou buoys, instead of those predicted using the WWIII model, were used to determine H_S at the toe of the seawall, and this H_S value was then used to estimate the wave run-up heights on Chi-Gu and Mi-Tou seawalls. Comparisons of measured and re-forecasted wave run-up heights on Chi-Gu and Mi-Tou seawalls by using various empirical run-up formulas are presented in Figs. 13 and 14. Equations (10) and (16) were used to estimate $Ru_{2\%}$ in Figs. 13 and 14, respectively.

Compared with Fig. 12, when observed wave data from nearby buoys are used as offshore waves in Figs. 13 and 14, agreement between the forecasted and measured run-up heights improves greatly, although discrepancies between both values remain. These discrepancies may

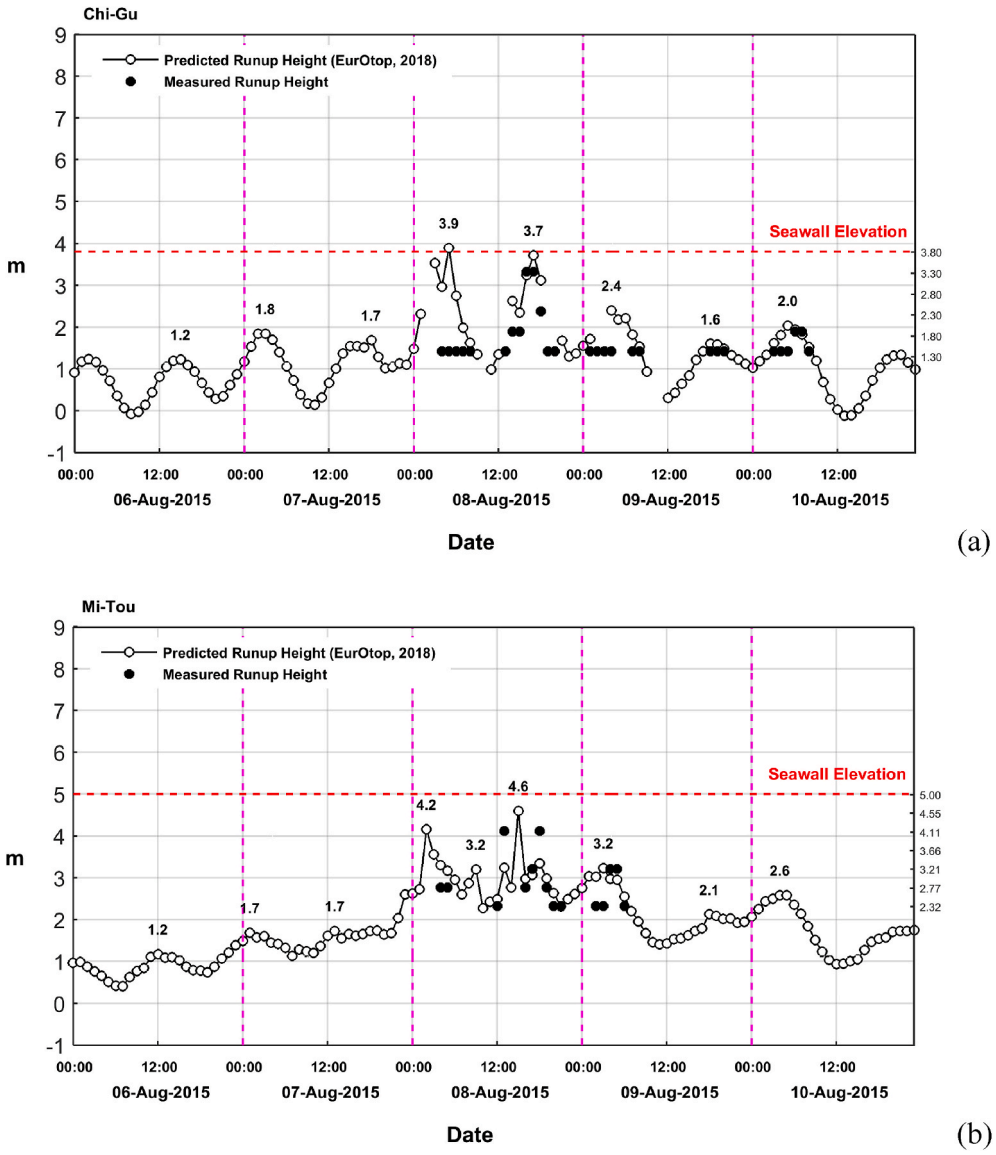

Fig. 14. Comparison of forecasted and measured hourly maximum wave run-up heights $Ru_{\max}$ at the (a) Chi-Gu seawall and (b) Mi-Tou seawall when measured wave data from nearby Chi-Gu and Mi-Tou data buoys were used as offshore wave conditions. The forecasted $Ru_{\max}$ was determined from $Ru_{2\%}$ estimated using Eq. (16).

have occurred because buoys are sufficiently far from seawalls such that the measured waves are not the same as the actual offshore waves to be used for determining the H_S at the toe of the seawall. In the case of the Tsen-Wen seawall, because the Chi-Gu buoy and seawall are near each other, the measured wave data resulted in adequate run-up estimates (Fig. 8 (b)). A comparison of results in Figs. 13 and 14 reveal that similar to Fig. 9, without the factor for a shallow foreshore γ_h, run-up heights obtained using Eq. (16) are higher than those obtained using Eq. (10), particularly when H_S values at the toe of the seawall are high.

To demonstrate the differences between the simulated and observed typhoon-induced ocean waves, Fig. 15 (a) presents a comparison of the H_S measured at the Chi-Gu buoy during the period of typhoon Soudelor with those predicted with the WWIII model by using the wind fields forecasted by the WRF, JMA, and NCEP weather models. The corresponding comparison of the mean wave period is depicted in Fig. 15 (b). Fig. 15 (c) shows the POM-predicted water level during the same typhoon period. Fig. 16 presents results similar to those in Fig. 15 but at the location of the Mi-Tou data buoy. Fig. 15 (a) indicates that as typhoon Soudelor was moving away from the southwestern coast of Taiwan on August 8, 2015, refer to Fig. 11, the difference between the simulated and measured H_S increased, especially from 04:00 to 21:00 on August 8, 2015, and the WWIII model apparently underestimated the ocean waves regardless of the wind field used. Except for this period, the simulated and measured H_S values agree well with each other. Similar to Fig. 8 (b), observed wave data for some hours were discarded because they did not satisfy the data quality criteria set by the COMC. A comparison of the simulated and measured mean wave periods, as illustrated in Fig. 15 (b), reveals that the difference between the two values increased in the same time period as that in Fig. 15 (a). A comparison of the simulated and measured wave data at the location of the Mi-Tou buoy, as illustrated in Fig. 16 (a) and (b), reveals similar characteristics as those illustrated in Fig. 15 (a) and (b).

The buoys deployed in the Chi-Gu and Mi-Tou waters belonged to the WRA, Taiwan, and were operated by the COMC. As depicted in Fig. 2, the Chi-Gu data buoy was located at (22°45′52″N, 120°09′52″E), and the Mi-Tou data buoy was located at (23°05′41″N, 120°00′19″E). The Chi-Gu buoy was located on the northwestern side of the Chi-Gu seawall at a distance of approximately 7.3 km from the seawall, and the Mi-Tou buoy was located on the southwestern side of the Mi-Tou seawall at a distance of approximately 6.6 km from the seawall. The floating data buoys measured air pressure, air temperature, wind speed and direction, water temperature, wave height and direction, and current speed and

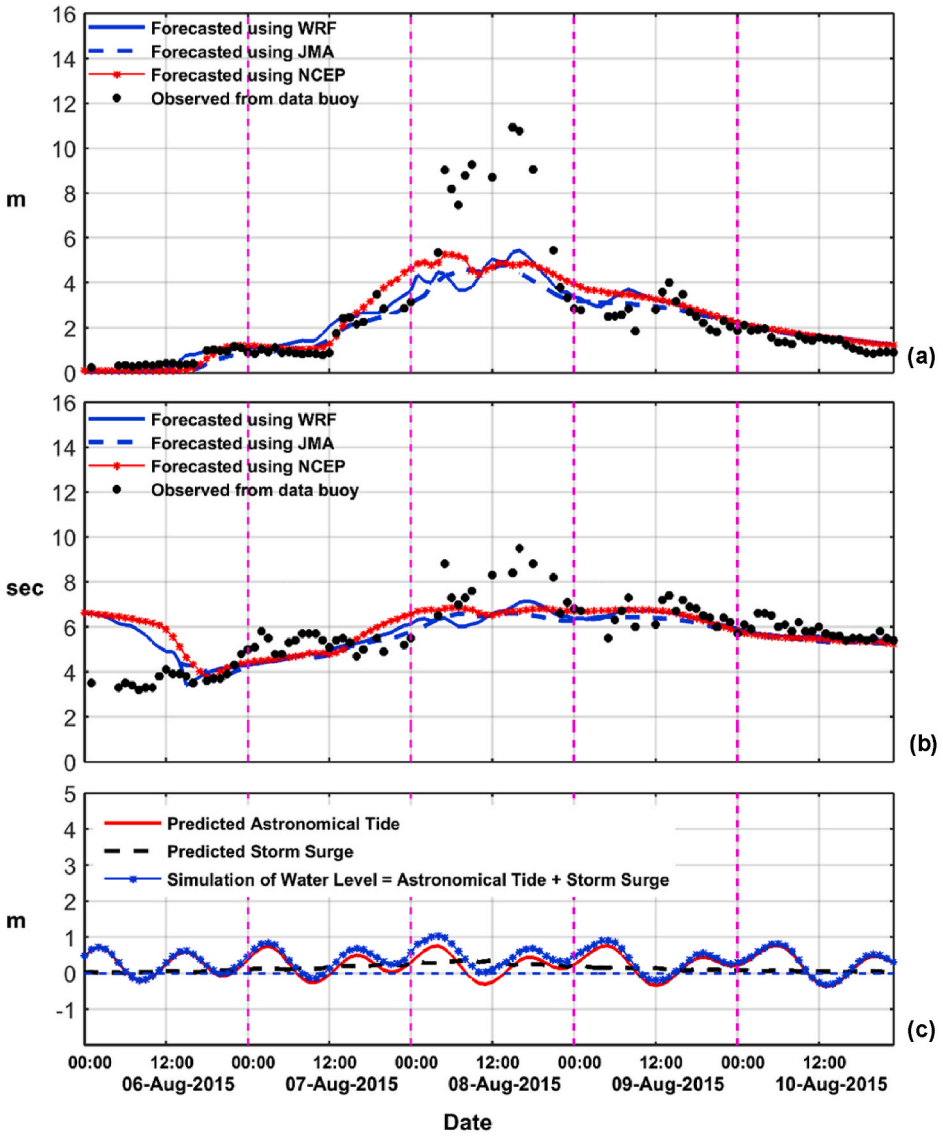

Fig. 15. Comparison of offshore wave data measured at the Chi-Gu buoy during typhoon Soudelor with those predicted using the WWIII model at the buoy site by using various wind fields in terms of (a) significant wave height and (b) mean wave period. (c) Water levels at the buoy site predicted using POM.

direction. The measurements were recorded according to an hourly update cycle, with a measurement duration of 10 min and sampling rate of 2 Hz. The accuracy of the monitored significant wave height, mean wave period, and directional wave spectrum obtained using these buoys was verified through comparison with the values determined from the water surface elevations monitored with a Global Navigation Satellite System (GNSS) buoy (Lin et al., 2017).

A comparison of the wave run-up heights during the typhoon periods shown in Fig. 8 (a), 10 (a) and 12 suggests that the unsatisfactory forecasting of run-up heights in Fig. 12 may be attributable to the inaccurate offshore wave data obtained using the WWIII model under storm conditions. However, the wave data obtained using the same wave model seem to have provided accurate forecasts of run-up heights, as depicted in Fig. 8 (a) and 10 (a). Therefore, the inaccurate offshore wave data may be ascribed to the inaccurate wind fields provided by the weather model.

4.3. Run-up heights on the Chi-Gu seawall during typhoons Meranti and Malakas in 2016

In 2016, typhoons Meranti and Malakas hit Taiwan in rapid succession. The paths of these two typhoons are illustrated in Fig. 17 (a) and (b). As summarized in Table 2, typhoon Meranti was a strong typhoon with a radius of 220 km at a wind scale of 7. Typhoon Malakas was a moderate-strength typhoon with a radius of 180 km at a wind scale of 7. Typhoon Meranti was near Taiwan from 18:00 on September 13 to 12:00 on September 14, and typhoon Malakas was close to the southern waters of Taiwan from 06:00 on September 16 to 00:00 on September 17. Because the paths of the two typhoons did not pass through the island, on the basis of discussion in Section 4.2, we expected accurately forecasted run-up heights. Fig. 18 presents a comparison of the forecasted and measured run-up heights at the Chi-Gu seawall from September 13 to 17. In Fig. 18 (a) and (b), $Ru_{2\%}$ values were estimated using Eqs. (10) and (16), respectively. As discussed in Sections 4.1 and 4.2, without the factor for a shallow foreshore γ_h, run-up heights obtained using Eq. (16) were higher than those obtained using Eq. (10), particularly when $1 \leq h/H_S \leq 4$. Fig. 18 (b) indicates that the run-up heights were overestimated from 18:00 to 22:00 on September 14, 2016, when typhoon Meranti moved to the western side of the Chi-Gu seawall.

Fig. 18 (a) reveals that forecasted wave run-up heights coincided with measured data. Although the path of typhoon Meranti did not pass through the island, its center touched the southernmost tip of Taiwan.

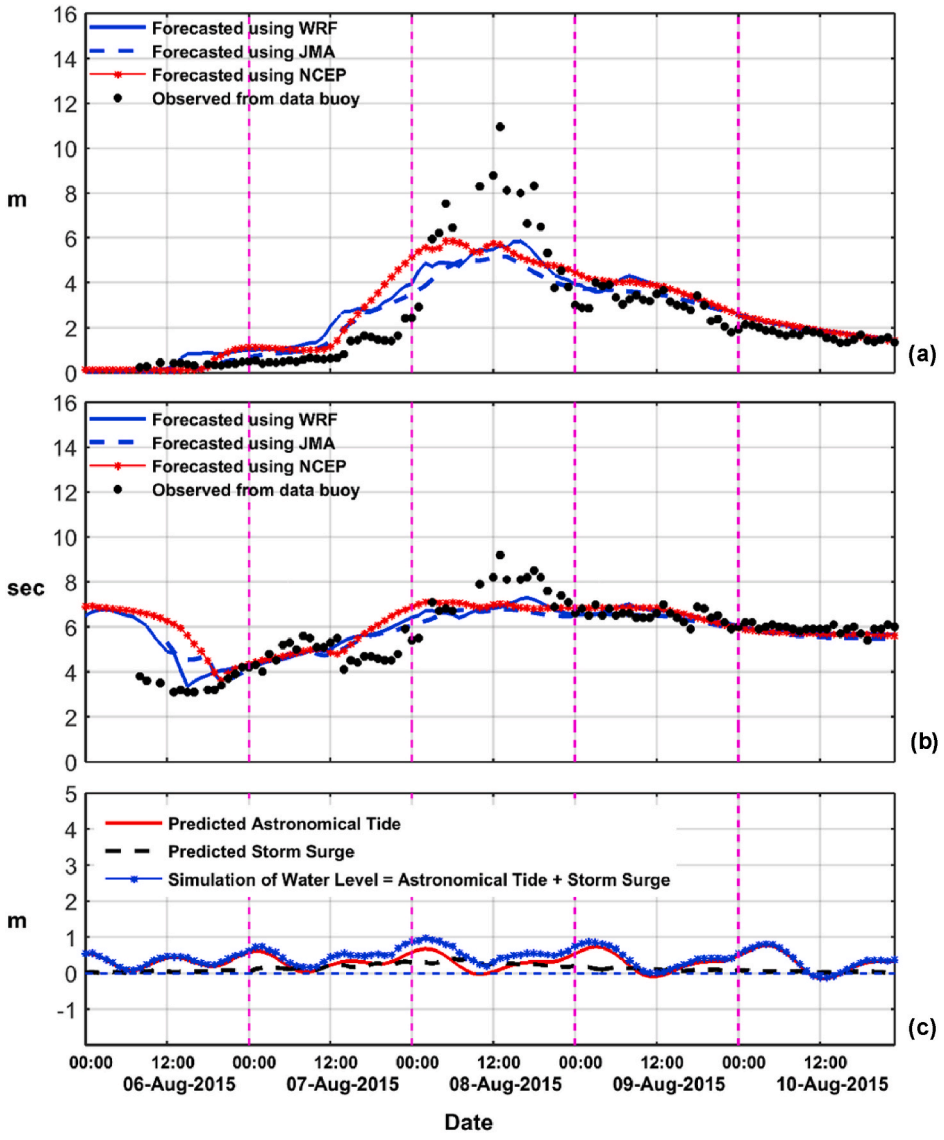

Fig. 16. Comparison of offshore wave data measured at the Mi-Tou buoy during typhoon Soudelor with those predicted using the WWIII model at the buoy site by using various wind fields in terms of (a) significant wave height and (b) mean wave period. (c) Water levels at the buoy site predicted using POM.

Because the radius of typhoon Meranti at the wind scale of 7 was 220 km and the north-to-south length of the island of Taiwan is approximately 400 km, the structure of this typhoon was severely affected by the topography of the island when it approached Taiwan. As mentioned, topographic effects increase the uncertainty associated with predicting wind fields and induce large deviations in forecasted wind fields when various wind models are applied. Large deviations in wind fields cause large variations in predicted ocean waves and wave run-up heights. This phenomenon was evident in the wider band of run-up heights from 12:00 on September 14 to 00:00 on September 15. By contrast, although typhoon Malakas was near the southern waters of Taiwan from 00:00 on September 16 to 00:00 on September 17, it remained far from the island. Consequently, the topography of the island only marginally affected the typhoon, and ocean waves predicted using various wind models were approximately the same. Therefore, these predictions produced range of wave run-up heights with a narrow band from 00:00 on September 16 to 00:00 on September 17, as illustrated in Fig. 18 (a) and (b).

The aforementioned characteristics of predicted ocean waves during typhoons Meranti and Malakas are illustrated in Fig. 19, in which measured offshore waves from the Chi-Gu buoy are compared with predicted ones obtained using various wind fields. In Fig. 19, NCEP wind fields produced the most accurate ocean wave predictions among the three weather models. Because the path of typhoon Meranti touched the southernmost tip of Taiwan, the forecasted typhoon path also affected the wind field predictions. This may explain why wind fields from various weather models produced different ocean wave predictions, especially those from 12:00 to 23:00 on September 14, when typhoon Meranti was near the southernmost tip of Taiwan. Furthermore, because higher offshore waves obtained from NCEP wind fields more closely approximated to measured ones, the measured Ru_{max} values were close to the upper limits of the forecasted run-up band (Fig. 18 (a)).

4.4. Inaccuracies of the wave run-up forecasting model

The wave run-up forecasting model proposed in this study was established on the basis of the procedure detailed in Fig. 3. Inaccuracies involved in the procedure in Fig. 3 are summarized as follows:

(i) Inaccuracies in forecasted wind fields obtained from the NCEP, JMA, and WRF weather models.
(ii) Inaccuracies in predicted water levels and ocean waves obtained from POM and WWIII models, respectively.

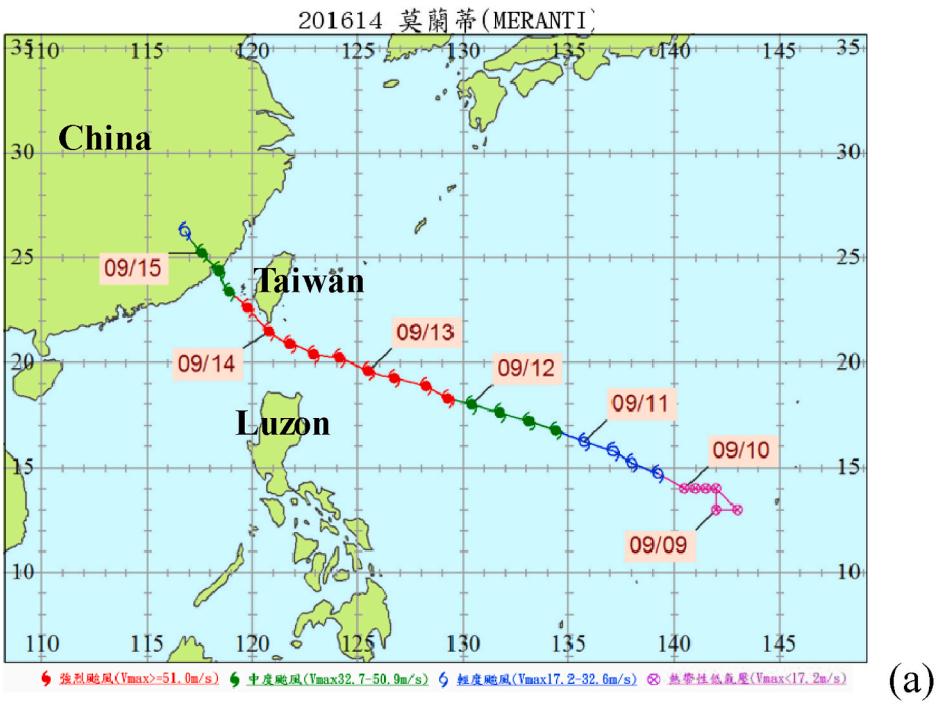

Fig. 17. (a) Path of typhoon Meranti that passed through south Taiwan on September 14, 2016; (b) path of typhoon Malakas that passed over the eastern waters of Taiwan
(Data source: https://www.cwb.gov.tw)..

(iii) An inaccuracy in Goda's empirical formula (Eq. (2)), which was used to determine the significant wave height at the toe of the seawall.
(iv) Inaccuracies in Eqs. (10) and (16) and associated unknown factors, such as γ_r, γ_β, and γ_h, for estimating $Ru_{2\%}$.
(v) An inaccuracy in estimating the $Ru_{\max}$ from $Ru_{2\%}$.
(vi) The bathymetry in front of the seawall is dynamic and constantly changing. Accordingly, inaccuracies occur if the bathymetry is not timely updated.

Because of these inaccuracies, the possibilities of errors in forecasting the wave run-up on seawalls warrant discussion.

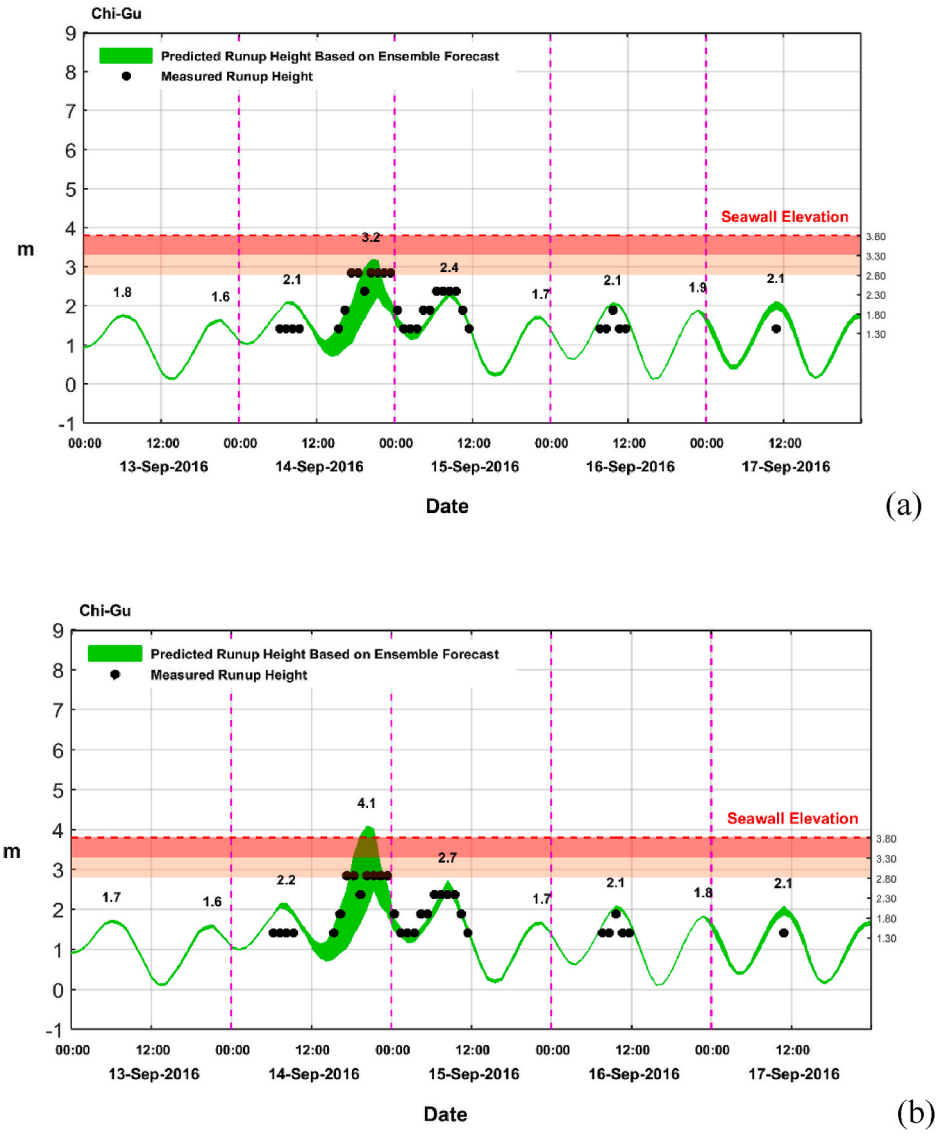

Fig. 18. Comparison of forecasted and measured hourly maximum wave run-up heights Ru_{max} on the Chi-Gu seawall during typhoons Meranti and Malakas. The forecasted Ru_{max} was determined from $Ru_{2\%}$ estimated using (a) Eq. (10) and (b) Eq. (16). The marked numbers on the right vertical axis of the lower figure denote the elevations of run-up sensors.

The inaccuracies in (i) and (ii) can be identified by comparing predicted and measured water levels and ocean waves. As demonstrated in this study, inaccuracies involved in (i) and (ii) are the main sources of forecast errors. The inaccuracy in (iii) can be identified by comparing H_S values at the toe of the seawall calculated from measured offshore waves using Eq. (2) with measured values. Inaccuracies in (iv) should be relatively minor because the formulas and associated factors were obtained from a large set of laboratory and field test data. The equation for determining Ru_{max} from $Ru_{2\%}$ was obtained based on the assumption that the wave run-up height has a Rayleigh distribution similar to the wave height distribution. This assumption may not be true if wave breaking occurs, thereby causing an inaccuracy in (v). The inaccuracy in (vi) can be avoided by using up-to-date bathymetry in front of the seawall.

Instead of these inaccuracies, the comparison of forecasted and measured Ru_{max} values on three seawalls during five typhoons that occurred from 2013 to 2016 in Taiwan revealed that the proposed model provides reliable forecasts of run-up heights on seawalls during the typhoon period, except for the poor forecasts obtained during typhoon Soudelor in 2015. These poor forecasts were attributed to that typhoon Soudelor passed through the island of Taiwan. Taiwan's mountainous topography makes accurate wind field forecasting difficult, particularly when typhoon passes through the island. To improve the unsatisfactory forecasting, the forecasted run-up heights were presented as a band with upper and lower limits as opposed to single values.

In this study, the observed and forecasted wave run-up did not overtop seawalls. When wave overtopping occurs, information on mean overtopping discharge or maximum overtopping volume becomes important for understanding possible coastal flooding. Van der Meer and Janssen (1995) proposed empirical formulas for determining mean overtopping discharge. EurOtop (2018) also provided detailed information on tolerable mean discharge and formulas for determining average overtopping discharge and overtopping volume for various seawalls.

5. Conclusions

In this study, the authors developed an operational real-time wave run-up monitoring system and a model for forecasting the wave run-up height on seawalls. These two approaches were combined to provide

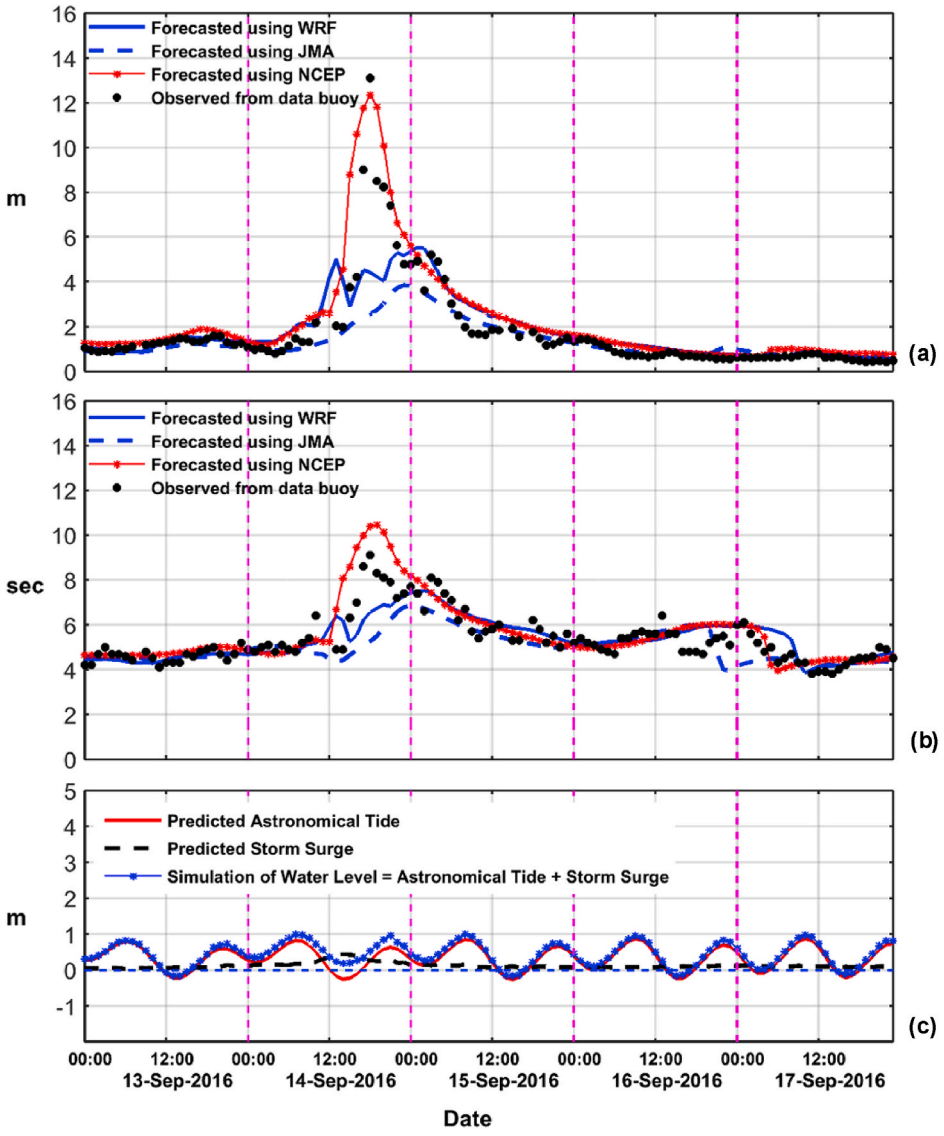

Fig. 19. Comparison of offshore wave data measured at the Chi-Gu buoy with those predicted using the WWIII model at the buoy site by using various wind fields during typhoons Meranti and Malakas in terms of (a) significant wave height and (b) mean wave period. (c) Water levels at the buoy site predicted using POM.

operational monitoring and forecasting of wave run-up on seawalls.

Several electrical conductivity sensors were installed on the seaward slopes of seawalls to measure the wave run-up heights. A GPRS module was used to transmit the monitoring data in real time to the desired remote locations. The monitoring system was set up on three seawalls, namely the Tsen-Wen, Chi-Gu, and Mi-Tou seawalls along the southwestern coast of Taiwan, to examine the capability of the forecasting model, especially during typhoon periods.

The POM and the WWIII model were used to provide 72-h forecasts of hourly water levels and ocean waves, respectively. The empirical formulas recommended in the Coastal Engineering Manual (2011) and EurOtop (2018) were adopted to estimate the wave run-up height.

In cases where a typhoon did not hit the island of Taiwan directly, such as the typhoons Trami and Usagi in 2013 and typhoon Malakas in 2016, the forecasted wave run-up heights on the studied seawalls agreed very well with the measured ones.

When a typhoon passed through the island, the forecasted wave run-up heights deviated from the measured ones. However, if the measured wave data from the nearby buoys were adopted as the offshore wave conditions rather than those obtained using the WWIII model, agreement between the forecasted and measured run-up heights is greatly improved.

To improve the uncertainties in predicted ocean waves caused by the forecasted wind field, the multi-model ensemble approach was adopted to obtain three ocean waves as ensemble members by using three weather models, namely the NCEP, JMA, and WRF models. Instead of using statistical analysis to produce the wave ensemble from the available members, the authors of this work used the ensemble members to obtain the upper and lower limits of the possible wave run-up heights. The forecasted wave run-up height was then represented as a band with a lower and an upper limit.

The good agreement between the forecasted and measured wave run-up heights under storm conditions indicates that the proposed approach can be used for operational forecasting of wave run-up on real seawalls, except when a typhoon hits the island of Taiwan directly.

Because wave conditions at the toe of seawall are crucial for the run-up estimate, wave monitoring near or at the toe of seawall, which was not performed in this study, is strongly recommended in future research.

CRediT authorship contribution statement

Dr. Ching-Jer Huang contributes to the supervision, writing - review

& editing. Mr. Yu-Cheng Chang, Mr. Shih-Chieh Tai, and Dr. Chun-Yuan Lin contribute to the wave run-up forecasting. Dr. Yen-Pin Lin and Dr. Chi-Min Chiu contribute to the wave run-up monitoring on the seawall. Dr. Yang-Ming Fan provides the water levels and ocean wave data using POM and WWIII. Dr. Li-Chung Wu studies the statistical features of the empirical wave run-up formulas.

Declaration of competing interest

The authors declare that they have no known competing financial interests or personal relationships that could have appeared to influence the work reported in this paper.

Acknowledgments

This study was jointly funded by the Water Resources Agency (WRA), the Ministry of Economic Affairs, Taiwan, under Contract Nos. 6 MOEAWRA102004 and MOEAWRA1030013 and by the Ministry of Science and Technology, Taiwan, under Contract No. MOST 108-2625-*M*-006-010. We would like to thank the Sixth River Management Office of the WRA for providing the bathymetry and geometry of the studied seawalls located at the southwestern coast of Taiwan. Moreover, the authors are very grateful to the Central Weather Bureau, Taiwan, for providing the forecasted wind fields. The authors are also grateful to the Editor-in-Chief and anonymous reviewers for their helpful comments and suggestions.

Appendix A. Supplementary data

Supplementary data to this article can be found online at https://doi.org/10.1016/j.coastaleng.2020.103750.

References

Ahrens, J., 1977. Prediction of Irregular Wave Runup. CETA 77-2. Coastal Engineering Research Center, U.S. Army Engineer Waterways Experiment Station, Vicksburg, Miss. (July).

Atkinson, A.L., Power, H.E., Moura, T., Hammond, T., Callaghan, D.P., Baldock, T.E., 2017. Assessment of runup predictions by empirical models on non-truncated beaches on the south-east Australian coast. Coast. Eng. 119, 15–31.

Battjes, J.A., 1971. Runup distributions of wave breaking on slopes. J. Waterw. Harbors, Coast. Eng. Division, ASCE 97, 91–114. No. WW1, Proc. Paper 7923.

Battjes, J.A., 1974. Wave Runup and Overtopping. Technical Advisory Committee on Protection Against Inundation, Rijkswaterstaat, The Hague, Netherlands.

Blumberg, A.F., Mellor, G.L., 1987. A description of a three-dimensional coastal ocean circulation model. In: Heaps, N.S. (Ed.), Three Dimensional Coastal Ocean Models, Coastal and Estuarine Sciences, vol. 4. American Geophysical Union, Washington, D. C., pp. 1–16

Bradford, S.F., 2011. Nonhydrostatic model for surf zone simulation. J. Waterw. Port, Coast. Ocean Eng. 137 (1), 163–174.

Carrier, G., Greenspan, H., 1958. Water waves of finite amplitude on a sloping beach. J. Fluid Mech. 4, 97–109.

Coastal Engineering Manual (CEM), 2011. Coastal Engineering Research Center, Report No. EM-1110-2-1100 (Part VI, Ch. VI-5). US Army Corps of Engineers, Washington DC, USA.

De Rouck, J., Van de Walle, B., Troch, P., Van der Meer, J., Van Damme, L., Medina, J.R., Willems, M., Frigaard, P., 2007. Wave run-up on the Zeebrugge rubble mound breakwater: full-scale measurement results versus laboratory results. J. Coast Res. 23 (3), 584–591.

De Waal, J.P., Van der Meer, J.W., 1992. Wave run-up and overtopping on coastal structures. In: Proc. 23rd Conf. Coast. Engrg., Venice, Italy, pp. 1758–1771.

EurOtop, 2007. Wave Overtopping of Sea Defenses and Related Structures: Assessment Manual August 2007. URL: www.overtopping-manual.com.

EurOtop, 2018. Manual on wave overtopping of sea defenses and related structures. An overtopping manual largely based on European research, but for worldwide application. Van der Meer, J.W., Allsop, N.W.H., Bruce, T., De Rouck, J., Kortenhaus, A., Pullen, T., Schüttrumpf, H., Troch, P. and Zanuttigh, B. www.overtopping-manual.com.

Fiedler, J.W., Brodie, K.L., McNinch, J.E., Guza, R.T., 2015. Observations of runup and energy flux on a low-sloped beach with high-energy, long-period ocean swell. Geophys. Res. Lett. 42 (22), 9933–9941.

Fiedler, J.W., Smit, P.B., Brodie, K.L., McNinch, J., Guza, R.T., 2018. Numerical modeling of wave runup on steep and mildly sloping natural beaches. Coast. Eng. 131, 106–113.

Goda, Y., 2010. Random Seas and Design of Maritime Structures, third ed. World Scientific Publishing Co. Pte. Ltd., p. 732

Hall, J.V., Watts, G.M., 1953. Laboratory Investigation of the Vertical Rise of Solitary Waves on Impermeable Slopes. Technical Memorandum No. 33, Beach Erosion Board. U.S. Army Corps of Engineers, Washington, DC.

Hordijk, D., 2004. Report on Field Measurements Petten Sea Defense, Storm Season 2003-2004 (RIKZ/2004.124w).

Hsiao, L.F., Chen, D.S., Kuo, Y.H., Guo, Y.R., Yeh, T.C., Hong, J.S., Fong, C.T., Lee, C.S., 2012. Application of WRF 3DVAR to operational typhoon prediction in Taiwan: impact of outer loop and partial cycling approaches. Weather Forecast. 27, 1249–1263.

Hsiao, S.C., Hsu, T.W., Lin, T.C., Chang, Y.H., 2008. On the evolution and run-up of breaking solitary waves on a mild sloping beach. Coast. Eng. 55, 975–988.

Hubbard, M.E., Dodd, N., 2002. A 2D numerical model of wave run-up and overtopping. Coast. Eng. 47, 1–26.

Hughes, S.A., 2004. Estimation of wave run-up on smooth, impermeable slopes using the wave momentum flux parameter. Coast. Eng. 51, 1085–1104.

Hunt, I.A., 1959. Design of seawalls and breakwaters. J. Wtrwy. and Harb. Div. 85, 123–152.

Kennedy, A.B., Chen, Q., Kirby, J.T., Dalrymple, R.A., 2000. Boussinesq modeling of wave transformation, breaking, and run-up. J. Waterw. Port, Coast. Ocean Eng. 126 (1), 39–47.

Komen, G.J., Cavaleri, L., Donelan, M., Hasselmann, K., Hasselmann, S., Janssen, P.E.A. M., 1994. Dynamics and Modelling of Ocean Waves. Cambridge University Press, p. 532.

Komen, G.J., Hasselmann, S., Hasselmann, K., 1984. On the existence of a fully developed wind-sea spectrum. J. Phys. Oceanogr. 14, 21–44.

Lin, Y.P., Huang, C.J., Chen, S.H., Doong, D.J., Kao, C.C., 2017. Development of a GNSS buoy for monitoring water surface elevations in estuaries and coastal areas. Sensors 17, 172. https://doi.org/10.3390/s17010172.

Longuet-Higgins, M., Stewart, R., 1964. Radiation stresses in water waves; a physical discussion with application. Deep Sea Res. Oceanogr. Abstr. 11 (4), 529–562.

Losada, I.J., Lara, J.L., Guanche, R., Gonzalez-Ondina, J.M., 2008. Numerical analysis of wave overtopping of rubble mound breakwaters. Coast. Eng. 55, 47–62.

Losada, M.A., Giménez-Curto, L.A., 1982. Mound breakwater under oblique wave attack, a working hypothesis. Coast. Eng. 6, 83–92.

Lynett, P.J., Wu, T.R., Liu, P.L.F., 2002. Modeling wave runup with depth-integrated equations. Coast. Eng. 46, 89–107.

Mase, H., 1989. Random wave runup height. J. Waterw. Port, Coast. Ocean Eng. 115 (5), 649–661.

Mazaheri, S., Ghaderi, Z., 2011. Shallow water wave characteristics in Persian Gulf. J. Coast Res. 64, 572–575.

Na, S.J., Do, K.D., Suh, K.-D., 2011. Forecast of wave run-up on coastal structure using offshore wave forecast data. Coast. Eng. 58, 739–748.

Pan, S.Q., Fan, Y.M., Chen, J.M., Kao, C.C., 2016. Optimization of multi-model ensemble forecasting of typhoon waves. Water Science and Eng 9, 52–57.

Pillai, K., Etemad-Shahidi, A., Lemckert, C., 2019. Wave run-up on bermed coastal structures. Appl. Ocean Res. 86, 188–194.

Power, J.G., Klemp, J.B., Skamarock, W.C., Davis, C.A., Dudhia, J., Gill, D.O., Coen, J.L., Gochis, D.J., Ahmadov, R., Peckham, S.E., Grell, G.A., Michalakes, J., Trahan, S., Benjamin, S.G., Alexander, C.R., Dimego, G.J., Wang, w., Schwartz, C.S., Romine, G. S., Liu, Z., Snyder, C., Chen, F., Barlage, M.J., Yu, W., Duda, M.G., 2017. The weather research and forecasting model: overview, system efforts, and future directions. Bull. Am. Meteorol. Soc. https://doi.org/10.1175/BAMS-D-15-00308.1.

Pritchard, D., Guard, P.A., Baldock, T.E., 2008. An analytical model for bore-driven run up. J. Fluid Mech. 610, 183–193.

Raichlen, F., Hammack, J., 1974. Run-up due to breaking and non-breaking waves. In: Proc. 14th Coast. Engrg. Conf. ASCE, Copenhagen, Denmark, pp. 1937–1955.

Ruju, A., Lara, J.L., Losada, I.J., 2014. Numerical analysis of run-up oscillations under dissipative conditions. Coast. Eng. 86, 45–56.

Saville, T., 1956. Wave run-up on shore structures. J. Wtrwy. and Harb. Div. 82 (2), 649–661.

Saville, T., 1962. An approximation of the wave runup frequency distribution. In: Proceedings of the Eighth Conference on Coastal Engineering, ASCE, Mexico City. Council on Wave Research, pp. 48–59.

Senechal, N., Coco, G., Bryan, K.R., Holman, R.A., 2011. Wave runup during extreme storm conditions. J. Geophys. Res. 116 (C7), C07032.

Shore Protection Manual, 1984. Coastal Engineering Research Center, U.S. Army Engineer Waterways Experiment Station, Vicksburg, Miss (Chap. 7).

Stockdon, H.F., Holman, R.A., Howd, P.A., Sallenger, A.H., 2006. Empirical parameterization of setup, swash, and runup. Coast. Eng. 53, 573–588.

Synolakis, C.E., 1987. The runup of solitary waves. J. Fluid Mech. 185, 523–545.

TAW, 2002. Wave Run-Up and Wave Overtopping at Dikes, Technical Report – Technical Advisory Committee for Flood Defense in the Netherlands (TAW) (Delft).

Tolman, H.L., 1991. A third generation model for wind waves on slowly varying, unsteady, and inhomogeneous depths and currents. J. Geophys. Res. 21, 782–797.

The WAVEWATCH III Development Group, 2016. User Manual and System Documentation of WAVEWATCH III Version 5.16. Tech. Note 329. NOAA/NWS/NCEP/MMAB, College Park, MD, USA, p. 326.

Troch, P., De Rouck, J., Van Damme, L., 1998. Instrumentation and prototype measurements at the Zeebrugge rubble mound breakwater. Coast. Eng. 35, 141–166.

Van der Meer, J.W., 1998. Wave run-up and overtopping. In: Pilarczyk, K.W. (Ed.), Dikes and Revetments: Design, Maintenance and Safety Assessment. AA Balkema, Rotterdam, The Netherlands), pp. 145–159.

Van der Meer, J.W., Janssen, J.P.F.M., 1995. Wave run-up and wave overtopping at dikes. In: Kobayashi, N., Demirbilek, Z. (Eds.), Wave Forces on Inclined and Vertical Wall Structures. ASCE, pp. 1–27.

Van der Meer, J.W., Stam, C.J.M., 1992. Wave run-up on smooth and rock slopes of coastal structures. J. Waterw. Port, Coast. Ocean Eng. 118 (5), 534–550.
Van Gent, M.R.A., 2001. Wave run-up on dikes with shallow foreshores. J. Waterw. Port, Coast. Ocean Eng. 127, 254–262.
Wenneker, I., Spelt, B., Peters, H., De Ronde, J., 2016. Overview of 20 years of field measurements in the coastal zone and at the Petten sea dike in The Netherlands. Coast. Eng. 109, 96–113.
Wu, Y.K., Hong, J.S., 2007. A literature review of wind forecasting technology in the world. IEEE Power Technology 504–509, 2007, Lausanne, July 1-5.
Yoo, J., Choi, J.Y., Yoon, J.J., Jun, K.C., Shim, J.S., Kim, S., Min, I.K., 2013. Remote sensing of wave run-up over breakwater slope in field using optical imagery. J. Coast Res. 65, 1451–1455.
Zou, Q.P., Chen, Y.P., Cluckie, I., Hewston, R., Pan, S.Q., Peng, Z., Reeve, D., 2013. Ensemble prediction of coastal flood risk arising from overtopping by linking meteorological, ocean, coastal and surf zone models. Q. J. R. Meteorol. Soc. 139, 298–313.